Copy No._____

Defence Research and Development Canada
Recherche et développement pour la défense Canada

DEFENCE R&D DÉFENSE

Three Dimensional Ship Hydrodynamic Coefficients Using the Zero Forward Speed Green Function

Kevin McTaggart

Defence R&D Canada

Technical Memorandum

DRDC Atlantic TM 2002-059

April 2002

Canada

Three Dimensional Ship Hydrodynamic Coefficients Using the Zero Forward Speed Green Function

Kevin McTaggart

Defence R&D Canada - Atlantic

Technical Memorandum

DRDC Atlantic TM 2002-059

April 2002

Author

Kevin McTaggart

Kevin McTaggart

Approved by

J.L. Kennedy
Head, Warship Performance

Approved for release by

K. Foster
Chair/Document Review Panel

Abstract

This report presents a method for predicting ship hydrodynamic coefficients and pressures in waves. Computations are performed in the frequency domain using the Green function for zero forward speed. Pressures and coefficients at non-zero forward speed are computed using extensions to zero speed results. The approach has been implemented using the Python programming language. The present implementation gives robust results over a wide range of wave frequencies. A new algorithm facilitates efficient computation of hydrodynamic terms for a large number of combinations of ship speed, heading, and incident wave frequency. Sample computations for the HALIFAX class demonstrate application of the method.

Résumé

Dans ce rapport, nous présentons une méthode de prédiction des coefficients hydrodynamiques et de la pression exercée sur un navire battu par la houle. Les calculs sont effectués dans le domaine des fréquences, à l'aide de la fonction de Green pour un navire dont la vitesse avant est nulle. Les pressions et les coefficients pour les vitesses avant non nulles sont calculés à partir d'extensions jusqu'aux résultats à l'arrêt. Nous avons programmé cette méthode avec le langage Python. Le programme actuel donne des résultats robustes pour une vaste gamme de fréquences de houle. Un nouvel algorithme facilite le calcul efficace des termes hydrodynamiques pour un grand nombre de combinaisons de vitesses de navire, de caps et de fréquences de la houle incidente. Pour illustrer l'utilisation de la méthode, nous présentons des calculs types pour des bateaux de la classe Halifax.

This page intentionally left blank.

Executive summary

Introduction

Strip theory is the most commonly used approach for computing ship motions and sea loads in waves. While computationally efficient, strip theory cannot give accurate hull pressure predictions, and has deteriorating accuracy as ship slenderness decreases. This report presents a three-dimensional method for computing hydrodynamic forces and pressures using the frequency domain Green function for zero ship speed. Forward speed effects are included using suitable approximations.

The present work is part of a larger effort to develop an object oriented software library for modelling and simulation of ship motions and sea loads in waves. This library will aim to incorporate capabilities that are currently spread among a number of existing codes, including SHIPMO7, PRECAL, and FREDYN.

Principal Results

The presented computational method gives robust and efficient computations of three-dimensional hydrodynamic coefficients. Using an 800 MHz Pentium III processor, sample radiation computations for the HALIFAX class require approximately ten seconds per encounter frequency when using a mesh with 225 panels on half of the wet hull. A new algorithm facilitates efficient computation of hydrodynamic terms for a large number of combinations of ship speed, heading, and incident wave frequency.

Significance of Results

The efficiency and robustness of the present three-dimensional approach indicates that it is a suitable replacement for strip theory. The three-dimensional method will likely give significantly improved accuracy for sea loads, which can be very sensitive to three-dimensional effects. The influence of three-dimensional effects becomes more important as ship slenderness decreases, suggesting that the present work will be particularly relevant to the KINGSTON class. In comparison to strip theory, the three-dimensional method also has the advantage of giving hull pressures.

Future Plans

The three-dimensional method will be incorporated into a new version of DRDC's SHIPMO program. The resulting program will build upon SHIPMO's unique strengths

in the areas of lift and viscous forces, which have been recently demonstrated by comparisons with full-scale trials and predictions from other ship motion codes.

Kevin McTaggart; 2002; Three Dimensional Ship Hydrodynamic Coefficients Using the Zero Forward Speed Green Function; DRDC Atlantic TM 2002-059; Defence R&D Canada - Atlantic.

Sommaire

Introduction

La méthode la plus couramment utilisée pour le calcul des mouvements des navires dans la houle et les forces qu'elle exerce sur eux est la théorie des bandes. Bien qu'efficace d'un point de vue numérique, elle ne permet toutefois pas de prédire précisément les pressions exercées sur la coque. Qui plus est, plus la coque est fine, moins les résultats de la méthode sont précis. Nous présentons dans ce rapport une méthode tridimensionnelle de calcul des forces et des pressions hydrodynamiques pour un navire ayant une vitesse nulle, qui utilise la fonction de Green dans le domaine des fréquences. Des approximations adéquates permettent de déduire les effets dus à la vitesse avant.

Ce travail fait partie d'un projet plus important visant à mettre au point une bibliothèque logicielle orientée-objet pour modéliser et simuler les mouvements des navires causés par la houle et les charges qu'elle exerce sur eux. Nous prévoyons inclure dans cette bibliothèque les capacités de calcul actuellement dispersées dans différents logiciels, notamment SHIPMO7, PRECAL et FREDYN.

Résultats principaux

La méthode que nous présentons permet d'effectuer des calculs robustes et efficaces des coefficients hydrodynamiques dans les trois dimensions. Sur un processeur Pentium III cadencé à 800 MHz, il faut environ dix secondes par fréquence incidente apparente pour effectuer des calculs pour une frégate de la classe Halifax simulée par une demi-coque immergée et modélisée par un réseau de 225 panneaux. Un nouvel algorithme facilite le calcul efficace des termes hydrodynamiques pour un grand nombre de combinaisons de vitesses de navire, de caps et de fréquences de houle apparente incidente.

Importance des résultats

Efficace et robuste, la méthode tridimensionnelle pourra remplacer convenablement la théorie des bandes. Nous croyons que la méthode tridimensionnelle améliorera grandement la précision des calculs des charges de mer, lesquelles dépendent fortement des effets tridimensionnels. Puisque l'impact de ces effets s'accroît avec la finesse de la coque des navires, le présent travail pourrait être très pertinent pour les navires de la classe Kingston. En outre, la méthode tridimensionnelle présente l'avantage de calculer les pressions sur la coque, ce que ne permet pas la théorie des bandes.

Plans pour l’avenir

On incorporera la méthode tridimensionnelle à la nouvelle version du logiciel SHIPMO de RDDC. Le programme résultant exploitera les capacités particulières du programme SHIPMO au chapitre des forces portantes et visqueuses, lesquelles ont été révélées lors de comparaisons avec les résultats d’essais en grandeur réelle et les prédictions d’autres programmes simulant les mouvements des navires.

Kevin McTaggart; 2002; Calcul des coefficients hydrodynamiques des navires dans les trois dimensions, à partir de la fonction de Green pour une vitesse avant nulle; DRDC Atlantic TM 2002-059; Defence R&D Canada - Atlantic.

Table of contents

List of tables

List of figures

1 Introduction

When evaluating the motions and loads acting on a ship in waves, solution of the oscillatory flow in the vicinity of the hull is a key element. Strip theory, which uses 2 dimensional approximations when solving the flow in the vicinity of a ship section, has been the most commonly used approach for solving motions and loads of a ship in waves. DRDC's SHIPMO7 [1] is an example of a strip theory code. Advances in computational power have made three-dimensional approaches practical for solving the oscillatory flow around a ship in waves. The Cooperative Research Ships code PRECAL [2] is an example of a three-dimensional ship motion code.

A recent comparison of measured motions with predictions for HMCS NIPIGON [3] indicates that SHIPMO7 gives very good motion predictions for a slender ship in moderately rough seas. In contrast, Version 4 of PRECAL gives good heave and pitch predictions but poor roll predictions. The ability of SHIPMO7 to give good lateral plane predictions is partially due to the work of Schmitke [4], who was among the first to consider the influence of lift forces on ship motion predictions. McTaggart [5] gives a more recent discussion of the influence of lift forces on ship motions and sea loads.

The strong predictions by DRDC's SHIPMO7 suggest it would be worthwhile to extend its capability to include three-dimensional hydrodynamic forces. This capability will improve the accuracy of predictions for low L/B vessels such as DND's KINGSTON class. Sea load predictions are particularly sensitive to three-dimensional effects, and will benefit from the present work. Three-dimensional hydrodynamic computations will also provide hydrodynamic pressures that can be used for structural analysis.

The present work is part of an effort to develop an object oriented library for ship motions and sea loads in waves, replacing the present FORTRAN code for DRDC's SHIPMO7. The move to object oriented software will contribute to code reuse, maintainability, and ease of integration to applications such as modelling and simulation.

This report describes a method for computing three dimensional hydrodynamic coefficients in the frequency domain using the Green function for zero forward speed. Section 2 describes the theory of hydrodynamic forces acting on a ship in waves. Section 3 describes the solution of hydrodynamic forces using a source distribution method. The solution procedure requires a panel representation of the ship hull, which is discussed in Section 4. Section 5 describes numerical implementation of the solution of the hydrodynamic forces. A new approach for efficient computation of hydrodynamic forces is presented in Section 6, followed by sample computations for the HALIFAX class in Section 7. Section 8 gives final conclusions.

2 Hydrodynamic Forces on a Ship in Waves

The hydrodynamic forces acting on a ship in waves are solved using potential flow theory. The present approach is similar to that used by many other investigators, including Beck and Loken [6], Papanikolaou and Schellin [7], and Hsiung and Huang [8].

The hydrodynamic forces are solved with respect to the ship centre of gravity; however, the coordinate system for the present report has its origin in the still waterplane aligned vertically with the ship centre of gravity (see Figure 1). The coordinate system translates with the steady forward speed of the ship. The reason for using a coordinate system not located at the CG is that many of the terms used for solving hydrodynamic forces are dependent on elevation relative to the still waterplane; thus, it is most convenient to use $z = 0$ for the still waterplane. Figure 2 gives the convention for sea direction.

The total oscillatory velocity potential in the vicinity of a floating body in waves is broken into components as follows:

$$\Phi(\vec{x},t) \;=\; \text{Real}\left\{\left[\phi_I(\vec{x},\beta,\omega_I)+\phi_D(\vec{x},\beta,\omega_I)+\sum_{j=1}^{6}\eta_j\phi_j(\vec{x},U,\omega_e)\right]e^{i\omega_e t}\right\} \quad (1)$$

where Φ is total velocity potential, $\vec{x}$ is location, t is time, Real $\{\ldots\}$ denotes the real part of the term in brackets, ϕ_I is incident wave velocity potential, β is relative sea direction, ω_I is incident wave frequency, ϕ_D is diffracted wave velocity potential, η_j is the complex motion amplitude for mode j, ϕ_j is radiation potential for mode j, and U is steady ship forward speed. The wave encounter frequency ω_e is given by:

$$\omega_e \;=\; |\omega_I \;-\; k_I\, U\;\cos\beta_s| \quad (2)$$

Deep water conditions are assumed, giving the following relationship for incident wavenumber:

$$k_I \;=\; \frac{\omega_I^2}{g} \quad (3)$$

Similarly, the wavenumber for radiated waves is given by:

$$k_e \;=\; \frac{\omega_e^2}{g} \quad (4)$$

The pressure at a point in the fluid is given by Bernoulli's equation for unsteady flow:

$$p \;=\; -\rho\left(\frac{\partial\Phi}{\partial t} \;+\; \frac{1}{2}\,|\nabla\Phi|^2 \;+g\,z\right) \quad (5)$$

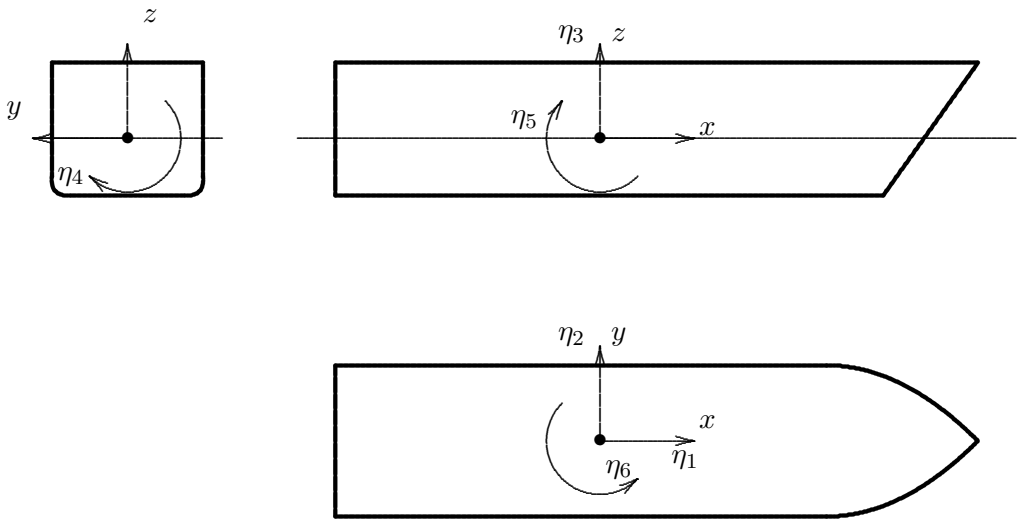

Figure 1: *Coordinate System for Solution of Hydrodynamic Forces*

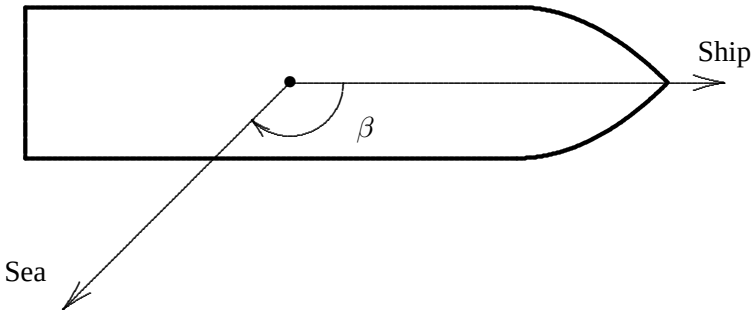

Figure 2: *Sea Direction for Solution of Hydrodynamic Forces*

where ρ is water density. Neglecting second and higher order terms, the oscillatory pressure acting on the ship hull is given by:

$$p \;=\; -\rho\left(i\,\omega_e \;-\; U\,\frac{\partial}{\partial x}\right)\left[\phi_I \;+\; \phi_D \;+\; \sum_{j=1}^{6}\eta_j\phi_j\right] \;-\; \rho g\zeta_3 \tag{6}$$

The last term of the above equation denotes the oscillatory pressure due to hydrostatic pressure, with ζ_3 being the oscillatory vertical displacement given by:

$$\zeta_3 \;=\; \eta_3 \;+\; y\eta_4 \;-\; x\eta_5 \tag{7}$$

The oscillatory motions of the ship can be solved as follows:

$$\left\{-\omega_e^2\left([M]+[A]\right) \;+\; i\omega_e[B] \;+[C]\right\}\;\{\eta\} \;=\; \left\{F^I \;+\; F^D\right\} \tag{8}$$

where $[M]$ is the ship mass matrix, $[A]$ is the added mass matrix, $[B]$ is the radiation damping matrix, $[C]$ is the hydrostatic stiffness matrix, $\left\{F^I\right\}$ is the incident wave force vector, and $\left\{F^D\right\}$ is the wave diffraction force vector. The added mass and damping matrix terms are given by:

$$A_{jk} \;=\; -\frac{\rho}{\omega_e}\int_{S_b}\left[\text{Imag}(\phi_k) \;-\; \frac{U}{\omega_e}\;\text{Real}\left(\frac{\partial\phi_k}{\partial x}\right)\right] n_j\;dS \tag{9}$$

$$B_{jk} \;=\; -\rho\int_{S_b}\left[\text{Real}(\phi_k) \;-\; \frac{U}{\omega_e}\;\text{Imag}\left(\frac{\partial\phi_k}{\partial x}\right)\right]\;n_j\;dS \tag{10}$$

where S_b denotes the surface of the ship. The normals for each motion mode k are given by:

$$n_1 \;=\; n_x \tag{11}$$

$$n_2 \;=\; n_y \tag{12}$$

$$n_3 \;=\; n_z \tag{13}$$

$$n_4 \;=\; yn_z - (z - z_{CG})n_y \tag{14}$$

$$n_5 \;=\; (z - z_{CG})n_x - xn_z \tag{15}$$

$$n_6 \;=\; xn_y - yn_x \tag{16}$$

where n_x, n_y, and n_z are the directional cosines for the unit normal pointing outward from the hull and z_{CG} is the height of the ship centre of gravity above the waterline. The wave excitation forces on the ship are given by:

$$F_j^I \;=\; \rho\,\omega_e\int_{S_b}\left(i\phi_I \;-\; \frac{U}{\omega_e}\;\frac{\partial\phi_I}{\partial x}\right) n_j\;dS \tag{17}$$

$$F_j^D \;=\; \rho\,\omega_e\int_{S_b}\left(i\phi_D \;-\; \frac{U}{\omega_e}\;\frac{\partial\phi_D}{\partial x}\right) n_j\;dS \tag{18}$$

3 Solution of Velocity Potentials Using Source Distribution Method

A source distribution method is used to solve for the radiation and diffraction potentials presented in the previous section. The radiated or diffracted velocity potential at a location in the fluid domain is expressed as follows:

$$\phi(\vec{x}) \;=\; \frac{1}{4\pi}\int_{S_b} G(\vec{x},\vec{x}_s)\;\sigma(\vec{x}_s)\;dS \tag{19}$$

where $\vec{x}_s$ is source location on the surface of the ship, $G(\vec{x},\vec{x}_s)$ is the Green function describing the flow at $\vec{x}$ caused by a source of unit strength at $\vec{x}_s$, and $\sigma(\vec{x}_s)$ is the strength of the source at $\vec{x}_s$. The Green function satisfies the continuity condition and all boundary conditions, with the exception of the following normal velocity boundary condition on the hull surface:

$$\frac{\partial\phi(\vec{x})}{\partial n} \;=\; v_n(\vec{x}) \text{ on } S_b \tag{20}$$

where $v_n(\vec{x})$ is the flow normal velocity on the hull surface. The source strengths are solved such that the following equation is satisfied:

$$-\frac{1}{2}\,\sigma(\vec{x}) \;+\; \frac{1}{4\pi}\int_{S_b}\frac{\partial G(\vec{x},\vec{x}_s)}{\partial n_{\vec{x}}}\,\sigma(\vec{x}_s)\;dS \;=\; v_n(\vec{x}) \text{ on } S_b \tag{21}$$

For radiation potentials, the hull boundary condition is:

$$\frac{\partial\phi_k(\vec{x})}{\partial n} \;=\; i\,\omega_e\,n_k \text{ on } S_b \tag{22}$$

For the wave diffraction potentials, the hull boundary condition is:

$$\frac{\partial\phi_D(\vec{x})}{\partial n} \;=\; -\,\frac{\partial\phi_I(\vec{x})}{\partial n} \text{ on } S_b \tag{23}$$

3.1 Velocity Potentials for Zero Forward Speed

Solution of the three-dimensional radiation and diffraction potentials for zero forward speed is discussed in detail by Faltinsen and Michelsen [9], Hogben and Standing [10], and Garrison [11]. The ship hull is discretized into N_p panels, and the source strength $\sigma(\vec{x}_s)$ is taken as being constant over each panel. The normal velocity boundary condition is satisfied at the centroid of each panel. Panel source strengths for each radiation mode and for wave diffraction are solved by satisfying the following:

$$\left\{\frac{\partial\phi}{\partial n}\right\} \;=\; [D]\;\{\sigma\} \tag{24}$$

where $[D]$ is the normal velocity influence matrix with terms given by:

$$D_{jk} \;=\; -\delta_{jk}\,\frac{1}{2} \;+\; \frac{1}{4\pi}\int_{S_k}\frac{\partial G(\vec{x}_j,\vec{x}_s)}{\partial n_{\vec{x}_j}}\,dS \tag{25}$$

where δ_{jk} is the Kroenecker delta function and S_k denotes the surface of panel k on the ship surface. Once the source strengths are solved, the potentials on the hull surface are given by:

$$\{\phi\} \;=\; [E]\;\{\sigma\} \tag{26}$$

where $[E]$ is the velocity potential influence matrix with terms given by:

$$E_{jk} \;=\; \frac{1}{4\pi}\int_{S_k} G(\vec{x}_j,\vec{x}_s)\,dS \tag{27}$$

The flow velocities in the x direction, which are required for the forward speed case, are given by:

$$\left\{\frac{\partial\phi}{\partial x}\right\} \;=\; [H]\;\{\sigma\} \tag{28}$$

where $[H]$ is the x velocity influence matrix with terms given by:

$$H_{jk} \;=\; -\delta_{jk}\,\frac{1}{2}\,n_{x-j} \;+\; \frac{1}{4\pi}\int_{S_k}\frac{\partial G(\vec{x}_j,\vec{x}_s)}{\partial x_{\vec{x}_j}}\,dS \tag{29}$$

3.2 Three-Dimensional Green Function for Zero Forward Speed in Deep Water

When solving the radiation and diffraction potentials, evaluation of the Green function is the most time consuming computational task. Many authors [9, 10, 11, 12, 13, 14] have written about its solution. Telste and Noblesse [15] have developed an efficient method that is commonly used for evaluating the Green function. Using the sign conventions in the present report, the Telste and Noblesse formulation of the Green function is:

$$G(\vec{x},\vec{x}_s,k_e) \;=\; \frac{1}{R} \;+\; \frac{1}{R_1} \;+\; \widetilde{G}_0(\vec{x},\vec{x}_s,k_e) \tag{30}$$

where R is the distance from the field point $\vec{x}$ to the source at $\vec{x}_s$, R_1 is the distance from the field point $\vec{x}$ to the image of the source at $\vec{x}_s$, and $\widetilde{G}_0$ is the frequency dependent term of the Green function. Garrison [11] discusses the Green function

at the zero and infinite frequency limits. The zero frequency (i.e., $k_e = 0$) limit is denoted $\overline{G}_0$ and given by:

$$\overline{G}_0(\vec{x}, \vec{x}_s, k_e) \;=\; \frac{1}{R} \;+\; \frac{1}{R_1} \text{ for } k_e = 0 \; (\omega_e = 0) \tag{31}$$

At infinite frequency (i.e., $k_e = \infty$), the Green function is denoted $\overline{G}_\infty$ and given by:

$$\overline{G}_\infty(\vec{x}, \vec{x}_s, k_e) \;=\; \frac{1}{R} \;-\; \frac{1}{R_1} \text{ for } k_e = \infty \; (\omega_e = \infty) \tag{32}$$

Accordingly, the frequency dependent portion $\widetilde{G}_0$ has the following limits:

$$\widetilde{G}_0(\vec{x}, \vec{x}_s, k_e) \;=\; 0 \;\text{ for } k_e = 0 \; (\omega_e = 0) \tag{33}$$

$$\widetilde{G}_0(\vec{x}, \vec{x}_s, k_e) \;=\; -\,\frac{2}{R_1} \;\text{ for } k_e = \infty \; (\omega_e = \infty) \tag{34}$$

Based on Telste and Noblesse, the frequency dependent term is expressed as follows:

$$\widetilde{G}_0(\vec{x}, \vec{x}_s, k_e) \;=\; 2\; k_e \; \left[\widetilde{R_0}(h, v) - i\; \pi \; J_0(h) \; \exp(v)\right] \tag{35}$$

where $\widetilde{R_0}(h, v)$ is a function to be evaluated and $J_0(h)$ is the Bessel function of the first kind of order zero. The function arguments h and v are as follows:

$$R_{xy} \;=\; \sqrt{(x - x_s)^2 \;+\; (x - x_s)^2} \tag{36}$$

$$h \;=\; k_e \; R_{xy} \tag{37}$$

$$v \;=\; k_e \; (z \;+\; z_s) \tag{38}$$

Thus, R_{xy} is the horizontal distance from a field point to a source, h is the non-dimensional horizontal distance, and v is the non-dimensional elevation of the field point relative to the image of the source.

The derivatives of the Green function are required for computing flow velocities induced by a source. The zero frequency portion of the Green function has the following derivatives,

$$\frac{\partial \overline{G}_0}{\partial x} \;=\; \frac{-(x - x_s)}{R^3} \;-\; \frac{(x - x_s)}{R_1^3} \tag{39}$$

$$\frac{\partial \overline{G}_0}{\partial y} \;=\; \frac{-(y - y_s)}{R^3} \;-\; \frac{(y - y_s)}{R_1^3} \tag{40}$$

$$\frac{\partial \overline{G}_0}{\partial z} \;=\; \frac{-(z - z_s)}{R^3} \;-\; \frac{(z + z_s)}{R_1^3} \tag{41}$$

Teltse and Noblesse give the following equations for the derivatives of the frequency dependent portion of the Green function

$$\frac{\partial \widetilde{G}_0}{\partial R_{xy}} = -2k^2 \left[\widetilde{R}_1(h,v) - i\pi J_1(h) \exp(v) \right] \quad (42)$$

$$\frac{\partial \widetilde{G}_0}{\partial x} = \frac{(x - x_s)}{R_{xy}} \frac{\partial \widetilde{G}}{\partial R_{xy}} \quad (43)$$

$$\frac{\partial \widetilde{G}_0}{\partial y} = \frac{(y - y_s)}{R_{xy}} \frac{\partial \widetilde{G}}{\partial R_{xy}} \quad (44)$$

$$\frac{\partial \widetilde{G}_0}{\partial z} = 2k^2 \left[\frac{1}{k_e \, R_1} + \widetilde{R}_0(h,v) - i\pi J_0(h) \exp(v) \right] \quad (45)$$

where $\widetilde{R}_1(h,v)$ is a function to be evaluated, and $J_1(h)$ is the Bessel function of the first kind of order one.

The majority of Telste and Noblesse's paper is devoted to the efficient solution of the terms $\widetilde{R}_0(h,v)$ and $\widetilde{R}_1(h,v)$, which will not be repeated here. The significance of Telste and Noblesse's work is demonstrated by its frequent citation in the literature, including a recent paper by Chakrabarti [14] confirming the accuracy of their approach.

3.3 Radiation Velocity Potentials for Non-Zero Forward Speed

For computational efficiency, velocity potentials for non-zero forward speed are determined from velocity potentials for zero forward speed. Beck and Loken [6], Papanikolaou and Schellin [7] and Salvesen et al. [16] have also used this approach. Once the velocity potentials at zero forward speed have been solved, velocity potentials at non-zero forward speed are:

$$\phi_1(U,\omega_e) = \phi_1(0,\omega_e) \quad (46)$$

$$\phi_2(U,\omega_e) = \phi_2(0,\omega_e) \quad (47)$$

$$\phi_3(U,\omega_e) = \phi_3(0,\omega_e) \quad (48)$$

$$\phi_4(U,\omega_e) = \phi_4(0,\omega_e) \quad (49)$$

$$\phi_5(U,\omega_e) = \phi_5(0,\omega_e) + \frac{U}{i\omega_e} \phi_3(0,\omega_e) \quad (50)$$

$$\phi_6(U,\omega_e) = \phi_6(0,\omega_e) - \frac{U}{i\omega_e} \phi_2(0,\omega_e) \quad (51)$$

The x derivatives of the forward speed potentials can be easily evaluated using the x derivatives of the zero speed potentials.

It should be emphasized that the speed correction terms given in this report are approximations, and are based on the assumption of U/ω_e being small. When considering the influence of ship speed using Equations (9), (10), (17), (18), (50) and (51), computations showed that motion predictions became unreliable for large U/ω_e. In practice, an upper limit should likely be imposed upon U/ω_e when performing computations. Motion predictions presented in Section 7 suggest that $L/2$ could be a suitable upper limit for U/ω_e.

Many investigators have developed more sophisticated and accurate approaches for incorporating forward speed effects in the frequency domain. Huang and Hsiung [17] discuss the influence of the scattered steady flow potential induced by the presence of the ship hull. Inglis and Price [18] present a frequency domain Green function which incorporates forward speed effects and has been used extensively by others. Unfortunately, computation of the forward speed Green function is very computationally intensive. Among the various algorithms for computing the forward speed Green function, Ba and Guilbard's [19] is likely the most efficient and most commonly used.

3.4 Incident and Diffracted Wave Potentials

The complex velocity potential of a regular wave system is as follows:

$$\phi_I \;=\; \frac{i\ g\ a}{\omega_I}\ \exp\left[-i\ k_I\ (x\cos\beta\ -\ y\sin\beta)\right]\ \exp(k_I\ z) \tag{52}$$

where a is the incident wave amplitude. The above equation is based on the convention of the wave crest being at the $x-y$ origin at time $t=0$. Fluid velocities are given by the following derivatives:

$$\frac{\partial\phi_I}{\partial x} \;=\; a\ \omega_I\ \cos\beta\ \exp\left[-i\ k_I\ (x\cos\beta\ -\ y\sin\beta)\right]\ \exp(k_I\ z) \tag{53}$$

$$\frac{\partial\phi_I}{\partial y} \;=\; a\ \omega_I\ \sin\beta\ \exp\left[-i\ k_I\ (x\cos\beta\ -\ y\sin\beta)\right]\ \exp(k_I\ z) \tag{54}$$

$$\frac{\partial\phi_I}{\partial z} \;=\; i\ a\ \omega_I\ \exp\left[-i\ k_I\ (x\cos\beta\ -\ y\sin\beta)\right]\ \exp(k_I\ z) \tag{55}$$

The incident wave elevation is given by:

$$\zeta_I \;=\; a\ \exp\left[-i\ k_I\ (x\cos\beta\ -\ y\sin\beta)\right] \tag{56}$$

Knowing the incident wave potential and its derivatives, the diffracted wave potential is solved in a manner similar to that for the radiation potentials. It is assumed that the only influence ship forward speed has on incident and diffracted wave potentials is due to encounter frequency; however, ship forward speed influences resulting pressures and forces due to the term $U\ \partial\phi/\partial x$ in Equations (6), (17) and (18).

3.5 Evaluation of Influence Matrix Terms from Panel Sources

Garrison [11] gives a detailed discussion of evaluation of influence matrix terms for determing velocity potentials using panel sources. If a field point is in close proximity to a source panel, then the variation of the Green function term $1/R$ over the source panel must be considered. The variation of the term $1/R_1$ over the image source panel can also be significant if the field point is close to the image source; however, this situation is less common. Fortunately, the frequency dependent term $\widetilde{G}_0$ can usually be considered constant with location over the source panel.

Garrison gives equations for integrating $1/R$ and its derivatives from a source panel. Integration of $1/R$ from a source panel requires numerical integration over the length of each side of the source panel. When evaluating velocity potential at the centroid of a ship panel, the source potential from itself has a dominant effect due to $1/R$ being large. For a quadrilateral source panel, the integral $\int_{S_s} 1/R \, dS$ to the field point at its own centroid has the following analytical solution:

$$\int_{S_s} 1/R \, dS \;=\; 2\sqrt{\frac{A_s}{b}} \left\{ \ln\left[b \;+\; \sqrt{b^2+1} \right] \;+\; b \ln\left[\frac{1 \;+\; \sqrt{b^2+1}}{b} \right] \right\} \quad (57)$$

where b is the aspect ratio of the panel. Figure 3 shows relative errors in $\int_{S_s} 1/R \, dS$ versus panel aspect ratio for Simpson's rule using 11 points per side of the panel. The relative error is less than 0.001 for panel aspect ratios less than 4.4.

The velocity potential at a field point will be largely influenced by the $\int_{S_s} 1/R \, dS$ terms from nearby panels. Figures 4 and 5 show relative errors in computed values of $\int_{S_s} 1/R \, dS$ as a function of $R(\vec{x}, \vec{x}_{sc})$, the distance from the field point location $\vec{x}$ to $\vec{x}_{sc}$, the centroid of a square source panel. The assumed correct value for evaluating relative error is from numerical integration using Simpson's rule with 1001 points per side of the source panel. Figure 4 shows the case for field points normal to the centroid of the source panel, while Figure 5 shows the case for field points planar to the source panel. Figures 4 and 5 indicate that Simpson's rule using 11 points per side of the source panel gives excellent results. If the integral is approximated based on the value of $R(\vec{x}, \vec{x}_{sc})$, then the field point must be a distance of at least $3\sqrt{A_s}$ from the centroid of a square source panel for the relative error to be less than one percent.

The derivatives of $1/R$ integrated from a source panel can be evaluated analytically, with no need for numerical integration. Figures 6 and 7 show the relative errors when using the source centroid approximation for evaluating the derivatives of $1/R$ integrated from a source panel. The derivatives are important because they represent the velocity (when divided by 4π) induced by the $1/R$ term of the source

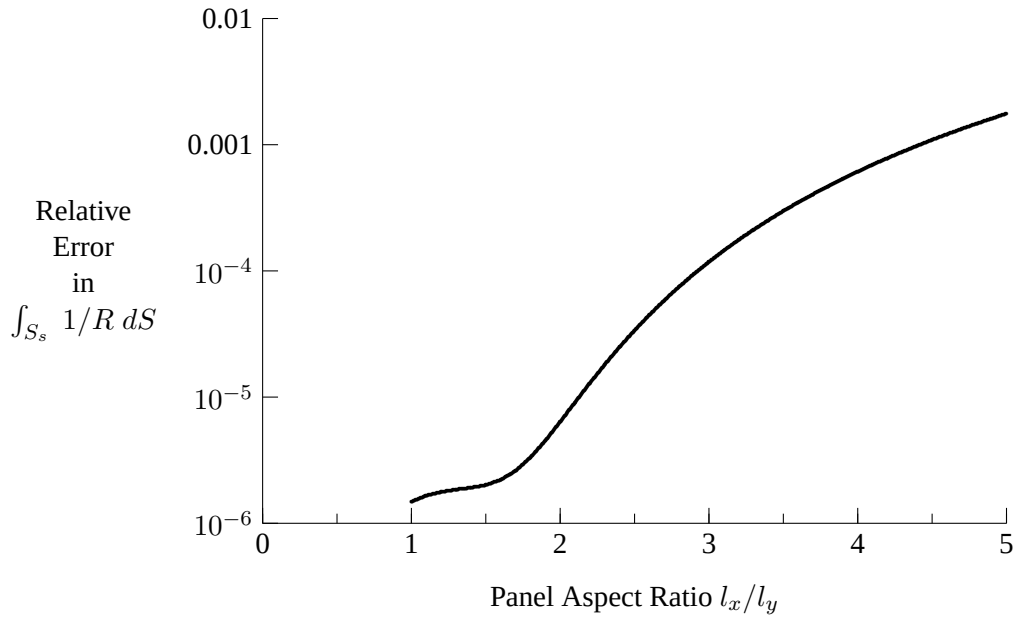

Figure 3: *Relative Error in Integration of Potential Term $\int_{S_s} 1/R\, dS$ from a Rectangular Source Panel to Own Centroid, Simpson's Rule with 11 Points per Side*

panel. The field point must be a distance of at least $5\sqrt{A_s}$ from the square source panel for the relative error to be less than one percent. It should be noted that $\partial(1/R)/\partial R$ is $-1/R^2$; thus, its magnitude decreases rapidly as R increases.

4 Panelling of Ship Hull for Seakeeping Calculations

The solution of the three-dimensional velocity potentials for a ship hull requires that the hull geometry be modelled using panels. Hess and Smith [20] is one of the earliest and most influential works on application of panel methods. Garrison [11] gives a comprehensive overview on application of panel methods to offshore structures in waves. At DRDC, Hally [21, 22, 23, 24] has done much work on panel methods for solving the steady flow around a ship hull.

For the present work, new software was developed for panelling a ship hull using input offsets. It was decided that developing new software would be easier than integrating existing software from Hally. Seakeeping computations require coarser hull descriptions than steady flow computations; thus, development of panelling software for the current application was relatively easy.

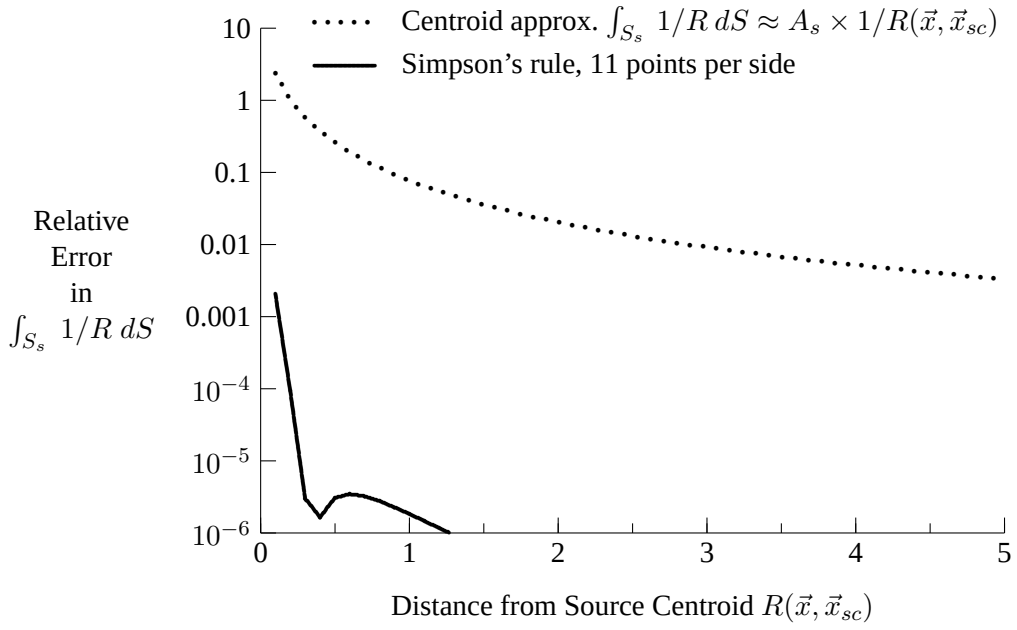

Figure 4: *Relative Error in Integration of $\int_{S_s} 1/R\, dS$ from 1 × 1 Source Panel to Normal Field Point*

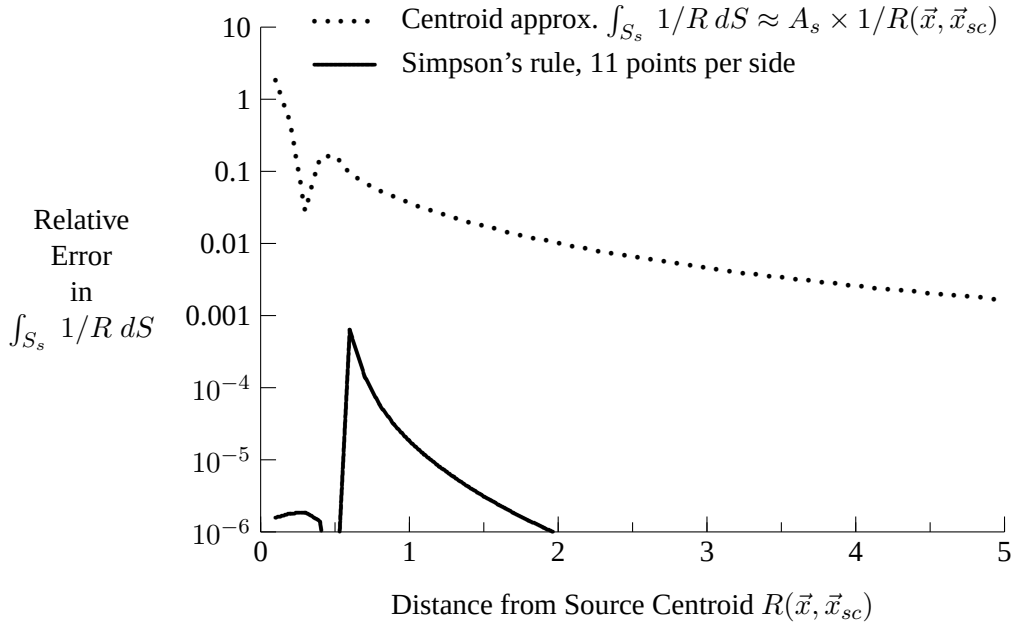

Figure 5: *Relative Error in Integration of $\int_{S_s} 1/R\, dS$ from 1 × 1 Source Panel to Field Point in Panel Plane*

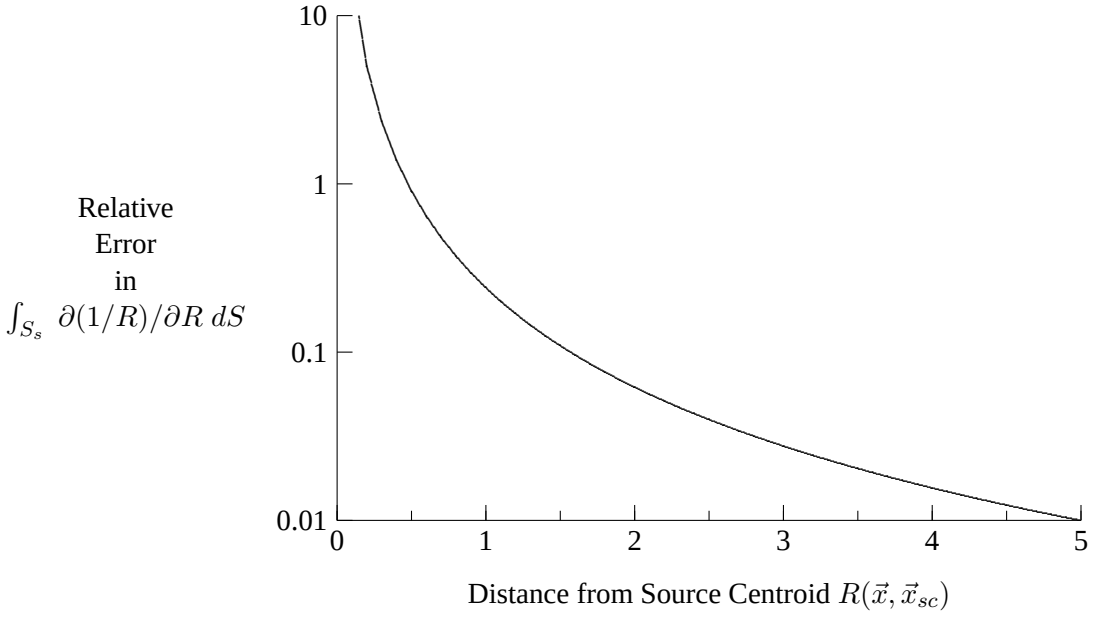

Figure 6: *Relative Error in Centroid Approximation for Integration of Velocity Term* $\int_{S_s} \partial(1/R)/\partial R \, dS$ *from 1 × 1 Source Panel to Field Point Normal to Panel*

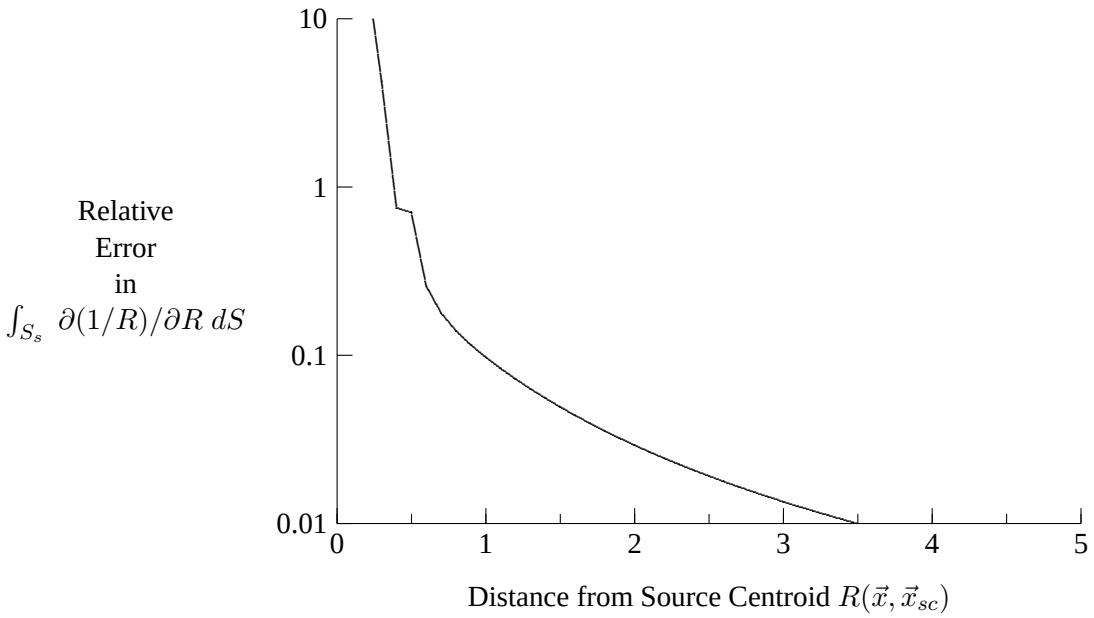

Figure 7: *Relative Error in Centroid Approximation for Integration of Velocity Term* $\int_{S_s} \partial(1/R)/\partial R \, dS$ *from 1 × 1 Source Panel to Field Point in Panel Plane*

Garrison gives useful guidelines for panelling of a body for computation of wave-induced forces. There should be a sufficient number of panels to adequately model the geometry of the body. Adjacent panels should be of similar size so that the source potential from a larger panel does not unduly influence adjacent smaller panels. Panel geometries should not be too elongated, with the upper limit on aspect ratio being approximately 5. In practice, the geometry of a ship hull can often be adequately described with 200 panels on each side of the hull.

Coordinates of panel vertices for a faired hull are easily generated from input ship offsets. If offsets are given for two ship sections, then longitudinal panels are generated girthwise from the keel to the waterline. The desired panel area and limit on aspect ratio will determine the number of panels in the longitudinal and girthwise directions. When generating panels between two sections, triangular panels can be used if the girth of one of the sections is zero (e.g., at the fore perpendicular).

Hess and Smith [20] describe evaluation of panel normals and centroids. For a triangular panel, the normal components are evaluated by taking the cross product of two of its edges and then applying a normalization factor. The centroid coordinates are merely the average of the coordinates of vertices. For a quadrilateral panel computed using four input vertices, the normal components are evaluated by taking the cross product of the two diagonals, thus yielding the rotational orientation of the panel plane. The location of the panel plane is fixed by specifying that it passes through the mean of the four vertex coordinates. Vertex coordinates are then adjusted to lie on the computed panel plane.

Hull hydrostatic properties can be computed from panel properties. For consistency between pressure and motion computations, the hydrostatic stiffness terms for a panelled hull should be computed using the panel properties. The volume of a panelled hull is determined by the following discretized equation:

$$\bigtriangledown \;=\; \sum_{j=1}^{N_p} A_j \; n_{z-j} \; z_j \tag{58}$$

where N_p is the total number of panels, A_j is the area of panel j, n_{z-j} is the z normal component of panel j, and z_j is the z value (relative to the waterline) of the centroid of panel j. The location of the centre of buoyancy relative to the waterline is:

$$z_{CB} \bigtriangledown \;=\; \sum_{j=1}^{N_p} A_j \; n_{z-j} \; \frac{1}{2} \; z_j^2 \tag{59}$$

The longitudinal centre of buoyancy, which corresponds with the longitudinal cen-

tre of gravity, is given by:

$$x_{CB} \bigtriangledown \;=\; \sum_{j=1}^{N_p} A_j \; n_{z-j} \; z_j \; x_j \tag{60}$$

For ship motion computations, x_{CB} is typically computed and then x coordinates are adjusted such that $x_{CB} = 0$. The hull waterplane area, which is used for computing heave stiffness, is given by:

$$A_{wp} \;=\; -\sum_{j=1}^{N_p} A_j \; n_{z-j} \tag{61}$$

The longitudinal centroid of floatation is given by:

$$x_{wp} \; A_{wp} \;=\; -\sum_{j=1}^{N_p} A_j \; n_{z-j} \; x_j \tag{62}$$

Waterplane moment terms are:

$$I_{wp-xx} \;=\; -\sum_{j=1}^{N_p} A_j \; n_{z-j} \; x_j^2 \tag{63}$$

$$I_{wp-yy} \;=\; -\sum_{j=1}^{N_p} A_j \; n_{z-j} \; y_j^2 \tag{64}$$

Using the above computed values, hydrostatic stiffness terms for motion equations are:

$$C_{33} \;=\; \rho \; g \; A_{wp} \tag{65}$$

$$C_{35} \;=\; -\rho \; g \; A_{wp} \; x_{wp} \tag{66}$$

$$C_{44} \;=\; \rho \; g \; [\bigtriangledown \; z_{CB} \; - \; \bigtriangledown \; z_{CG} \; + \; I_{wp-yy}] \tag{67}$$

$$C_{53} \;=\; C_{35} \tag{68}$$

$$C_{55} \;=\; \rho \; g \; [\bigtriangledown \; z_{CB} \; - \; \bigtriangledown \; z_{CG} \; + \; I_{wp-xx}] \tag{69}$$

5 Numerical Implementation for Solution of Velocity Potentials and Hydrodynamic Forces

The solution of velocity potentials and hydrodynamic forces has been implemented using the Python programming language [25, 26] and the Numeric Python extension library [27]. Python is a high level object oriented programming language. Its

syntax and capabilities are similar to C++ and Java; however, its high level nature leads to source code that is typically shorter and easier to read than C++ and Java.

5.1 Influence Matrices for Hull with Lateral Symmetry

It is assumed that the ship hull has lateral symmetry. Radiation potentials are evaluated only on the port side of the hull, while diffraction potentials are evaluated on both sides of the hull. Hull potential influence matrices are partitioned, leading to the following equations:

$$\left\{ \frac{\partial \phi^{port}/\partial n}{\partial \phi^{star}/\partial n} \right\} = \left[\begin{array}{c|c} D^{port,port} & D^{port,star} \\ \hline D^{star,port} & D^{star,star} \end{array} \right] \left\{ \frac{\sigma^{port}}{\sigma^{star}} \right\} \tag{70}$$

$$\left\{ \frac{\phi^{port}}{\phi^{star}} \right\} = \left[\begin{array}{c|c} E^{port,port} & E^{port,star} \\ \hline E^{star,port} & E^{star,star} \end{array} \right] \left\{ \frac{\sigma^{port}}{\sigma^{star}} \right\} \tag{71}$$

$$\left\{ \frac{\partial \phi^{port}/\partial x}{\partial \phi^{star}/\partial x} \right\} = \left[\begin{array}{c|c} H^{port,port} & H^{port,star} \\ \hline H^{star,port} & H^{star,star} \end{array} \right] \left\{ \frac{\sigma^{port}}{\sigma^{star}} \right\} \tag{72}$$

where the superscript $port$ denotes the port side of the hull and the superscript $star$ denotes the starboard side of the hull. Due to symmetry, the following relations exist:

$$\left[D^{port,port}\right] = \left[D^{star,star}\right] \tag{73}$$

$$\left[D^{port,star}\right] = \left[D^{star,port}\right] \tag{74}$$

$$\left[E^{port,port}\right] = \left[E^{star,star}\right] \tag{75}$$

$$\left[E^{port,star}\right] = \left[E^{star,port}\right] \tag{76}$$

$$\left[H^{port,port}\right] = \left[H^{star,star}\right] \tag{77}$$

$$\left[H^{port,star}\right] = \left[H^{star,port}\right] \tag{78}$$

$$\left\{\sigma_j^{port}\right\} = \left\{\sigma_j^{star}\right\} \text{ for } j = 1,3,5 \tag{79}$$

$$\left\{\sigma_j^{port}\right\} = \left\{-\sigma_j^{star}\right\} \text{ for } j = 2,4,6 \tag{80}$$

$$\left\{\phi_j^{port}\right\} = \left\{\phi_j^{star}\right\} \text{ for } j = 1,3,5 \tag{81}$$

$$\left\{\phi_j^{port}\right\} = \left\{-\phi_j^{star}\right\} \text{ for } j = 2,4,6 \tag{82}$$

where index j denotes the motion mode in the above equations. In the Python code, source strengths are determined by solving the following using the function LinearAlgebra.solve_linear_equations from the Numeric Python library:

$$\left[D^{port,port} + D^{port,star}\right] \left\{\sigma_j^{port}\right\} = \left\{\partial\phi_j^{port}/\partial n\right\} \text{ for } j = 1,3,5 \tag{83}$$

$$\left[D^{port,port} - D^{port,star}\right] \left\{\sigma_j^{port}\right\} = \left\{\partial\phi_j^{port}/\partial n\right\} \text{ for } j = 2,4,6 \quad (84)$$

$$\left[\begin{array}{c|c} D^{port,port} & D^{port,star} \\ \hline D^{port,star} & D^{port,port} \end{array}\right] \left\{\begin{array}{c} \sigma_D^{port} \\ \hline \sigma_D^{star} \end{array}\right\} = \left\{\begin{array}{c} -\partial\phi_I^{port}/\partial n \\ \hline \partial\phi_I^{star}/\partial n \end{array}\right\} \quad (85)$$

Once the source strengths are solved, the velocity potentials are computed by:

$$\left\{\phi_j^{port}\right\} = \left[E^{port,port} + E^{port,star}\right] \left\{\sigma_j^{port}\right\} \text{ for } j = 1,3,5 \quad (86)$$

$$\left\{\phi_j^{port}\right\} = \left[E^{port,port} - E^{port,star}\right] \left\{\sigma_j^{port}\right\} \text{ for } j = 2,4,6 \quad (87)$$

$$\left\{\begin{array}{c} \phi_D^{port} \\ \hline \phi_D^{star} \end{array}\right\} = \left[\begin{array}{c|c} E^{port,port} & E^{port,star} \\ \hline E^{port,star} & E^{port,port} \end{array}\right] \left\{\begin{array}{c} \sigma_D^{port} \\ \hline \sigma_D^{star} \end{array}\right\} \quad (88)$$

The x derivatives are computed in a similar manner.

A Python class HullRadDif has been created for solution of radiation and diffraction potentials of a symmetric ship hull. Upon class initialization, all zero and infinite frequency influence matrices are computed. Class methods are available for evaluating radiation potentials and hydrodynamic forces at specified encounter frequencies and ship speeds. Similarly, methods are available for evaluating diffraction potentials and incident wave forces at specified combinations of ship speed, relative wave heading, and wave frequency.

5.2 Evaluation of Frequency Dependent Portion of Green Function

When computing hull hydrodynamic forces in the frequency domain, most computational time is used for computing the frequency dependent portion of the Green function. Initial Python code for its evaluation was based on equations presented by Telste and Noblesse [15]. Subsequent code profiling revealed that the ascending series and Haskind algorithms presented in the equations were very slow. These formulations were re-written based on Fortran source code presented by Telste and Noblesse, which uses rational approximations that are not presented in the equations of their paper.

Python is an interpreted language, and is thus typically slower than compiled languages such as C++ and Fortran. Many Python library components, including much of Numeric Python, are written in C or C++ for improved performance. Lutz [25] gives details regarding calling C functions from Python. The frequency dependent version of the Green function was re-written in C and compiled using the C++ Builder 5 compiler. A basic version of this compiler is available from the Borland web site (http://www.borland.com/bcppbuilder/freecompiler/) at no cost.

5.3 Variation of Green Function from Panel Source

When evaluating the Green function and its derivatives from a panel source, the variation of terms $1/R$ and $1/R_1$ with location over the panel source is considered. The frequency dependent portion of the Green function $\widetilde{G}_0$ is assumed to be constant with location over the panel source. As mentioned previously, $\widetilde{G}_0$ approaches 0 at low frequencies and approaches $-2/R_1$ at high frequencies. To minimize the influence of the variation of $\widetilde{G}_0$ with location on a source panel, the method for evaluating the integral of the Green function from a source panel depends on the encounter frequency:

$$\begin{aligned} \int_{S_s} G(\vec{x},\vec{x}_s,k_e)\,dS &\approx \int_{S_s}\frac{1}{R}\,dS + \int_{S_s}\frac{1}{R_1}\,dS \\ &\quad + A_s\,\widetilde{G}_0(\vec{x},\vec{x}_{sc},k_e) \ \text{ for } \omega_e \le \omega_e^t \qquad (89) \\ \int_{S_s} G(\vec{x},\vec{x}_s,k_e)\,dS &\approx \int_{S_s}\frac{1}{R}\,dS - \int_{S_s}\frac{1}{R_1}\,dS \\ &\quad + A_s\left[\frac{2}{R_1(\vec{x},\vec{x}_{sc})} + \widetilde{G}_0(\vec{x},\vec{x}_{sc},k_e)\right] \ \text{ for } \omega_e > \omega_e^t \qquad (90) \end{aligned}$$

where $\vec{x}_{sc}$ is the location of the centroid of the source panel, and ω_e^t is a specified transition frequency that determines which of the above two equations is used. The derivatives of the Green function integrals are evaluated in a similar manner. Selection of a suitable transition frequency ω_e^t can be done empirically and will depend mainly on the size of the ship. The next section of this report shows that a transition frequency of 2.0 rad/s gives good results for the Canadian frigate HALIFAX.

When evaluating the $1/R$ integral terms, Simpson's rule with 11 points per side is used when the field point is close to the source. By default, the centroid approximation is used when $R > 5\sqrt{A_s}$; however, this value can be changed. Similarly, the centroid approximation is used for $1/R_1$ integral terms when $R_1 > 5\sqrt{A_s}$.

6 Efficient Computation of Hydrodynamic Terms for Seakeeping and Sea Loads Computations

Computation of three-dimensional ship hydrodynamic terms can be computationally intensive due to the large number of times that the Green function must be evaluated. The number of Green function evaluations for a symmetric hull will be:

$$N_G = 2\,N_p^{port}\,N_e \qquad (91)$$

where N_p^{port} is the number of panels on the port side of the hull and N_e is the number of encounter frequencies. A common approach is to evaluate the hull Green functions for the encounter frequency arising from each combination of ship speed, heading, and wave frequency. This approach can lead to a large number of encounter frequencies. An alternative approach would be to store hull Green functions for a range of encounter frequencies (e.g., 0.1, 0.2, . . ., 6.0 rad/s) and to use interpolation between stored Green functions; however, this approach would require a large amount of memory.

A new approach has been developed for efficient evaluation of radiation and diffraction potentials. The user provides an input range of encounter frequencies for radiation calculations. The user also provides ship speeds, headings, and wave frequencies for diffraction computations. Green functions and radiation potentials are solved for the lowest two encounter frequencies. Each combination of ship speed, heading, and wave frequency is then checked to see if the associated encounter frequency lies between the two encounter frequencies for which Green functions are currently stored, and linear interpolation of Green functions is used where appropriate. This process is repeated for all input encounter frequencies. Computed radiation potentials can be stored for all input encounter frequencies and computed diffraction potentials can be stored for all input combinations of ship speed, heading, and wave frequency. The accuracy of the interpolation procedure will depend on the intervals between input encounter frequencies. The input intervals should be sufficiently small to describe variations in added mass and damping for all modes of motion.

For encounter frequencies below and above the input encounter frequency range, the zero and infinite frequency Green functions (Equations (31) and (32)) are used for solving velocity potentials. Normalized velocity potentials $\phi/(i\omega_e)$ are evaluated and stored at the zero and infinite frequency limits in a manner similar to that used for 2D potentials in Reference 28.

The present computational procedure has been implemented into a Python class HullRadDiffDB, which is considered to be a database extension of the class HullRadDiff described earlier. Class HullRadDiffDB can take between several minutes and several hours to initialize, depending primarily of the number of seaways (i.e., number of combinations of ship speed, heading, and wave frequency) for diffraction computations. Once initialized, class HullRadDiffDB can quickly provide required potentials using interpolation of stored values.

7 Sample Computations for the HALIFAX Class

To verify implementation of the three-dimensional method, sample computations have been performed using the HALIFAX class frigate. Table 1 gives the ship configuration for the present computations, which is the same as for the sample case in the SHIPMO7 manual [1].

Table 1: *Main Particulars for HALIFAX Class Frigate*

Length, L	124.5 m
Beam, B	14.8 m
Midships draft, T_{mid}	5.025 m
Trim by stern, t_s	-0.135 m
Displacement, $\triangle$	4732 tonnes
Vertical centre of gravity, $\overline{KG}$	6.23 m
Dry roll radius of gyration r_{xx}	4.506 m
Dry pitch radius of gyration r_{yy}	29.815 m
Dry yaw radius of gyration r_{zz}	29.815 m

7.1 Hydrostatic Properties

Hull panels were generated from input offsets by specifying ship draft, trim, nominal panel area, and limiting panel aspect ratio. Three different panelled hulls were generated, with nominal panel areas of 5.0, 2.5, and 1.0 m^2. A maximum panel aspect ratio of 4.0 was specified for each hull. Figures 8 to 10 show the resulting meshes. The colour of each plotted panel is a function of its nominal elevation. Table 2 shows that hydrostatic properties have excellent agreement among the three different meshes, with the greatest relative difference being 0.7 percent for volumes between the coarse and fine meshes.

7.2 Added Mass and Damping Coefficients at Zero Forward Speed

Added mass and damping coefficients have been computed for HALIFAX at zero forward speed using the 3 different panel meshes. When computing frequency independent terms of influence matrices, the user supplies input parameters indicating

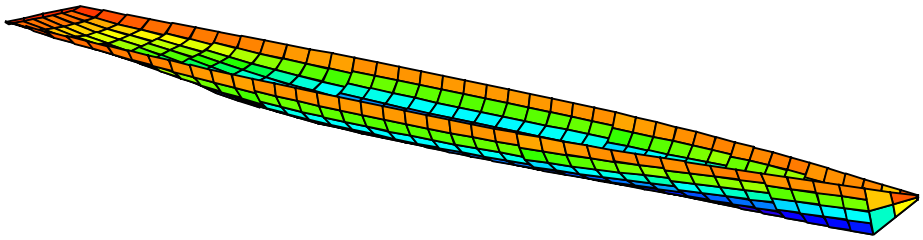

Figure 8: *Coarse Mesh for HALIFAX*

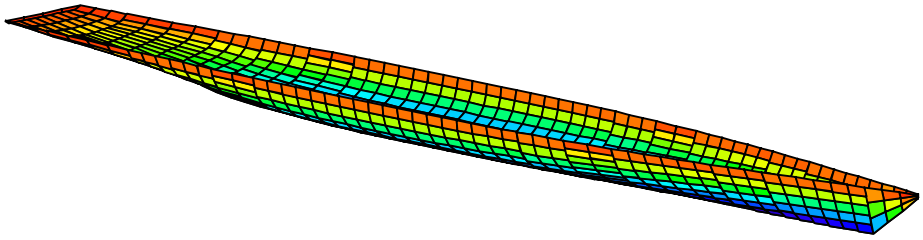

Figure 9: *Medium Mesh for HALIFAX*

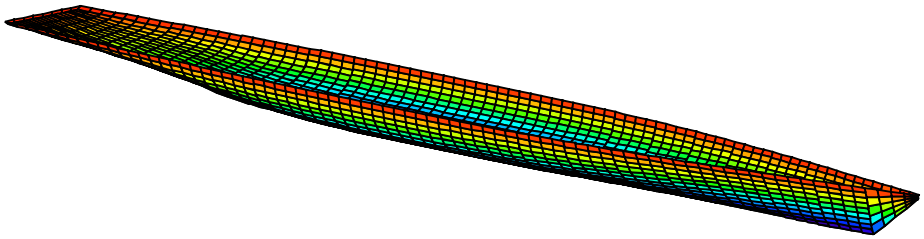

Figure 10: *Fine Mesh for HALIFAX*

Table 2: *Hydrostatic Properties for Different Panel Meshes*

	Coarse	Medium	Fine
Nominal panel size (m^2)	5.0	2.5	1.0
Number of panels on port side	225	428	1041
Volume (m^3)	4537.8	4562.1	4571.9
LCB aft of FP (m)	64.542	64.562	64.563
CB wrt waterline (m)	-1.906	-1.912	-1.916
Wetted surface area (m^2)	1980.3	1984.4	1985.9

nondimensional threshold distances specifying when the centroid approximation can be used for integrating potential from a source. For the present computations, the centroid approximation is used when $R^2(\vec{x}, \vec{x}_{sc}) > 25A_s$ when considering the $1/R$ term from a source. Similarly, the centroid approximation is used for the $1/R_1$ integral from a source image when $R_1^2(\vec{x}, \vec{x}_{sc}) > 25A_s$.

Figures 11 to 16 show computed added mass and damping coefficients for HALIFAX using a coarse mesh with 225 panels on the port side of the ship. The coefficients are nondimensionalized by the dry inertial force for each mode. Results are presented for transition encounter frequencies of zero and infinity, meaning that all Green function integrals for each line are based on either Equation (89) or Equation (90). For $\omega_e^t = \infty$, the computations will be more accurate in the lower frequency range. Conversely, the computations will be more accurate in the higher frequency range for $\omega_e^t = 0$. The results indicate definite differences in results at low and high frequency ranges. The most noticeable difference is that irregular frequency effects are less pronounced when using Equation (90) for evaluating Green function integrals. This result is expected because irregular frequency effects occur at higher encounter frequencies. The two different evaluation methods give very similar results at a frequency of 2.0 rad/s, indicating that this is a suitable value for ω_e^t when performing computations for HALIFAX.

Figures 17 to 22 show computed hydrodynamic coefficients for HALIFAX using 3 different mesh sizes. The transition frequency ω_e^t has a value of 2.0 rad/s for computations with all 3 meshes. For wave frequencies up to 1.8 rad/s, the coefficients show little sensitivity to mesh size. At higher frequencies, the coefficients show greater sensitivity to mesh size. This phenomenon is most likely due to the presence of irregular frequencies. Ando's method [29] suggests that the irregular frequencies for HALIFAX will have a lower bound of 1.6 rad/s. Results for the finest mesh size exhibit fewer irregularities, suggesting greater accuracy.

Hydrodynamic coefficients for HALIFAX approach their infinite frequency values in the upper range of presented frequencies. In this upper range, added mass varies little with encounter frequency and damping is effectively zero. It appears that the infinite frequency approximation can be used for frequencies above 6 rad/s for HALIFAX. In the lower frequency range, the zero frequency approximation is suitable for frequencies below 0.1 rad/s.

In comparison with the two dimensional coefficients results presented by McTaggart [28], the most noticeable difference is that the present heave added mass coefficients approach finite values at lower frequencies. This difference could significantly influence computed motions and sea loads at lower encounter frequencies.

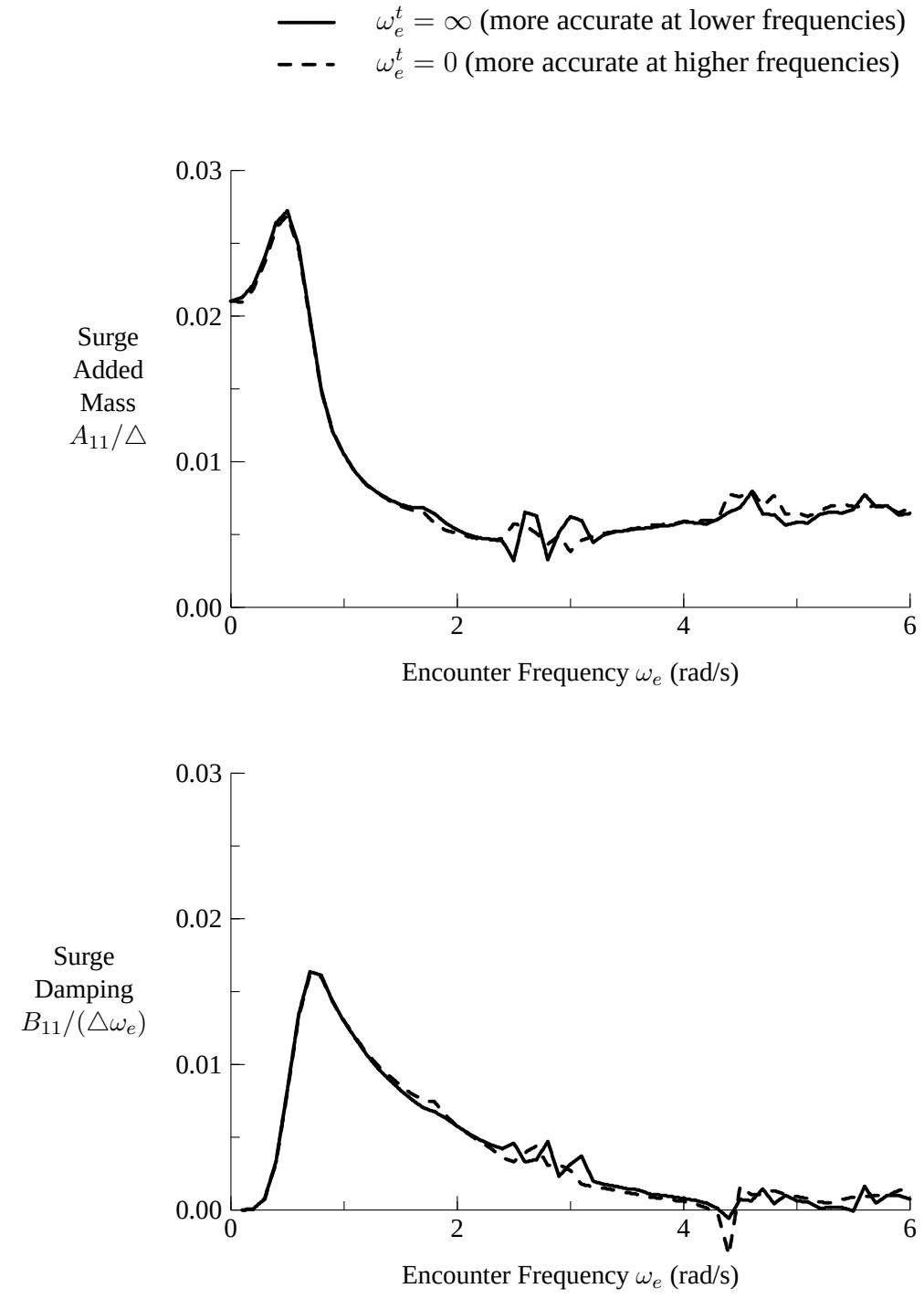

Figure 11: *Surge Added Mass and Damping Coefficients for Coarse Mesh HALIFAX*

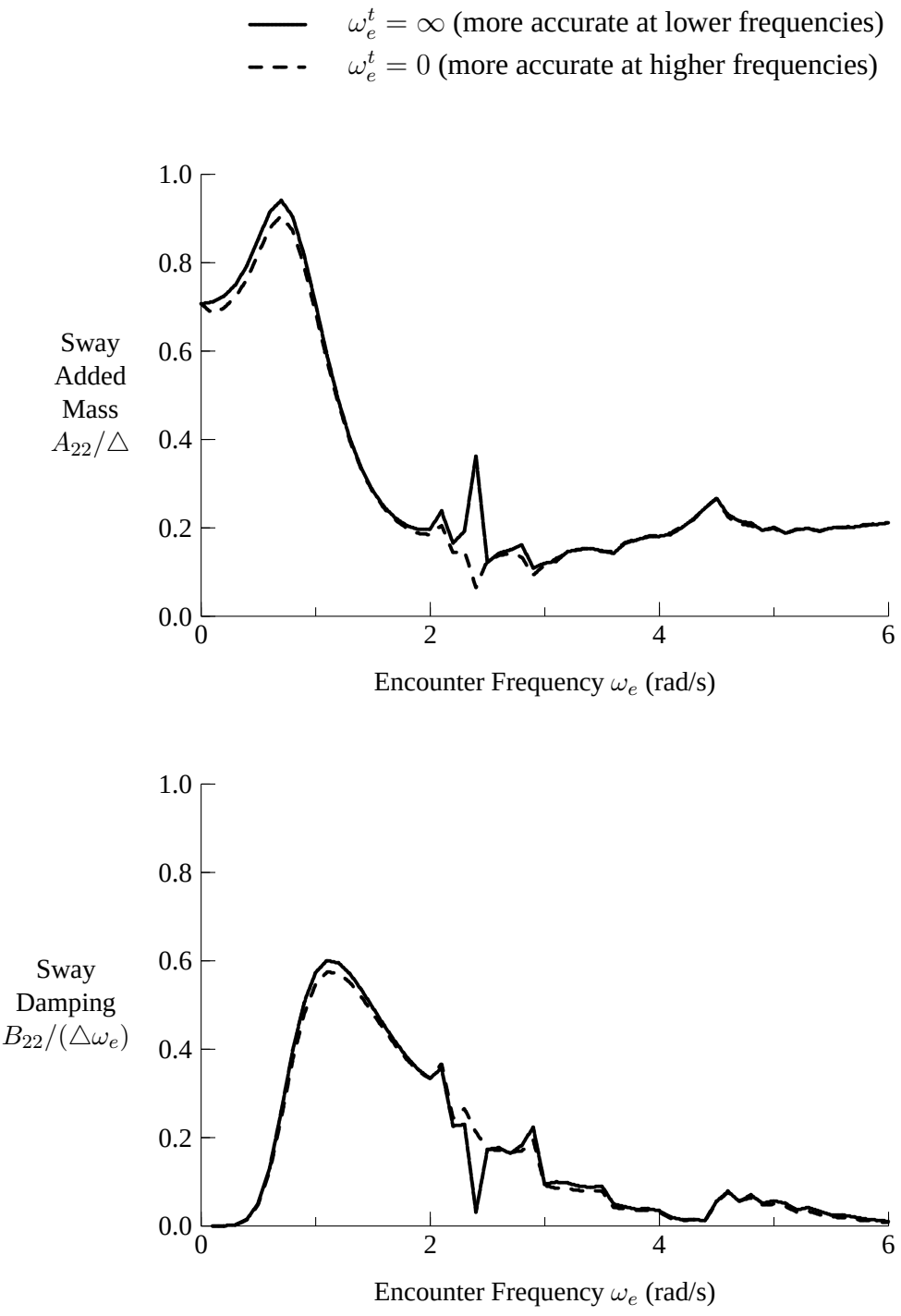

Figure 12: *Sway Added Mass and Damping Coefficients for Coarse Mesh HALIFAX*

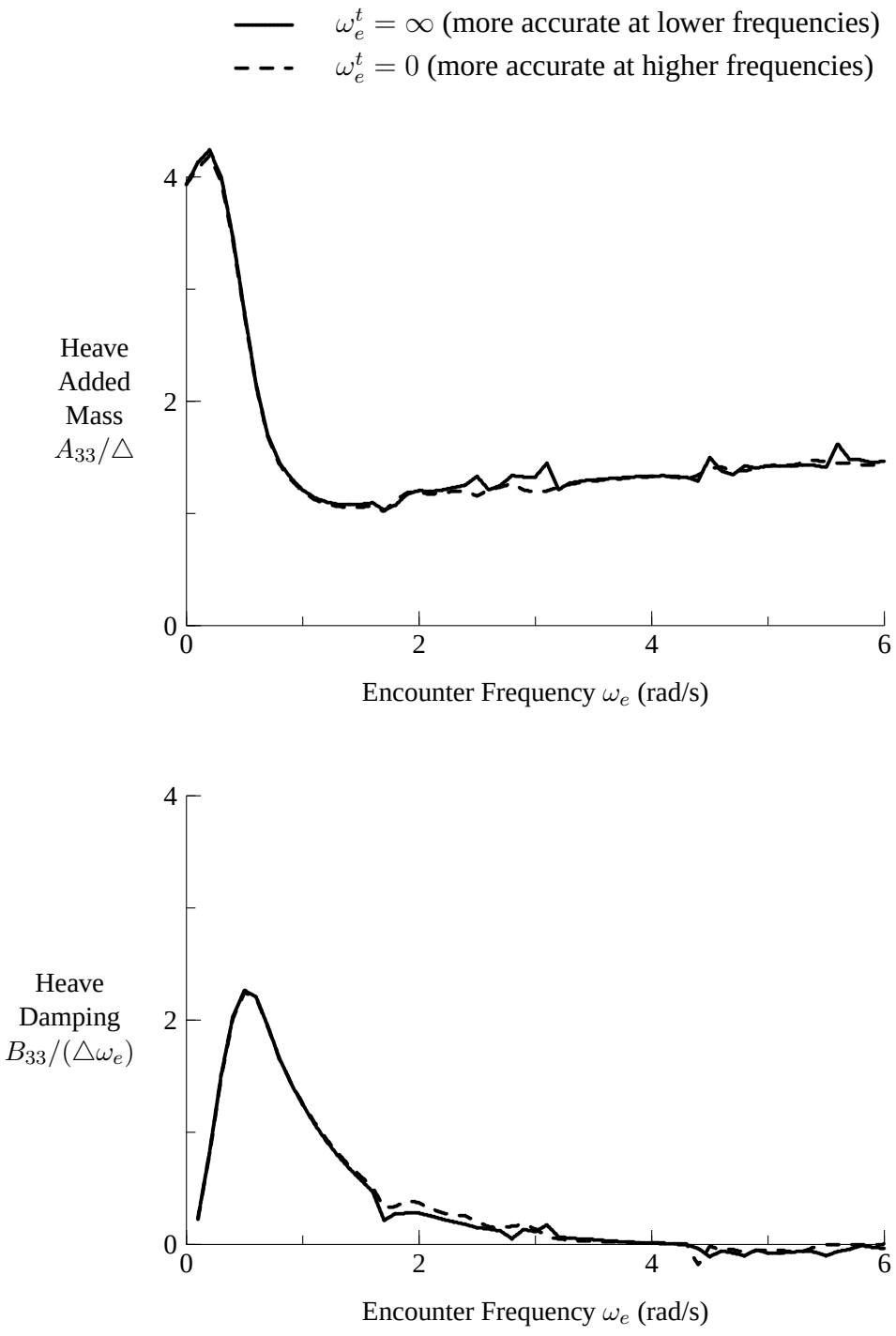

Figure 13: *Heave Added Mass and Damping Coefficients for Coarse Mesh HALIFAX*

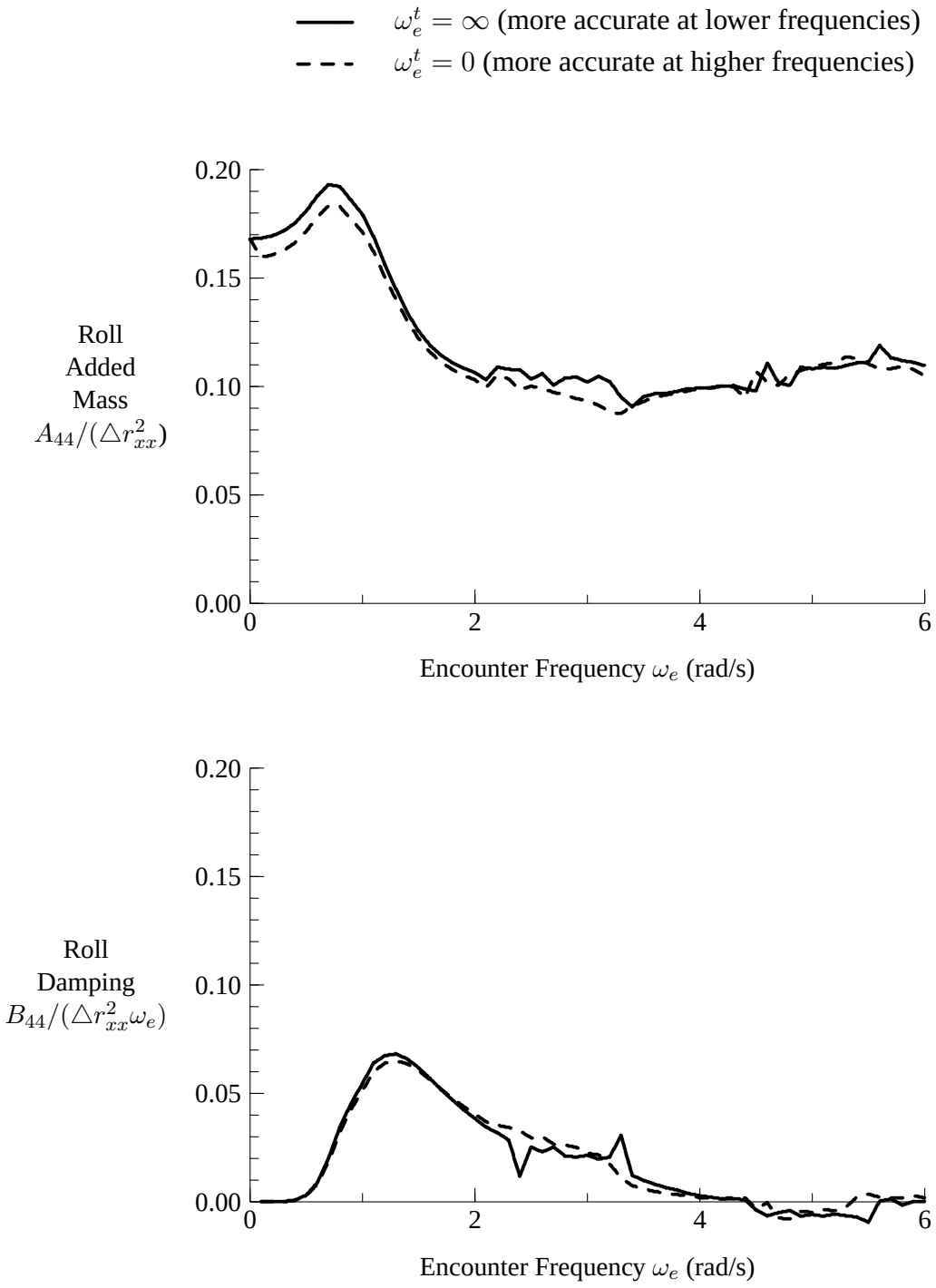

Figure 14: *Roll Added Mass and Damping Coefficients for Coarse Mesh HALIFAX*

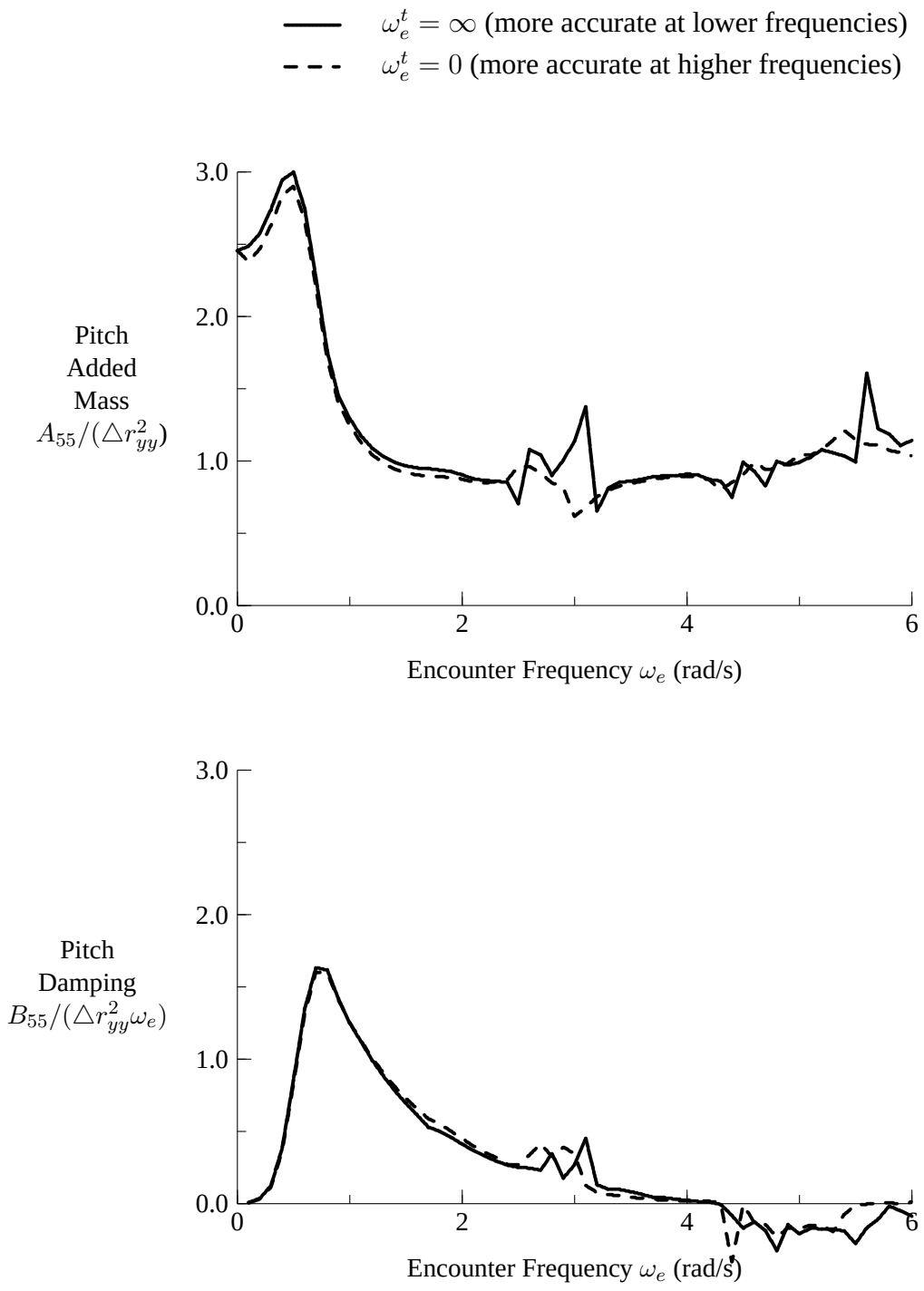

Figure 15: *Pitch Added Mass and Damping Coefficients for Coarse Mesh HALIFAX*

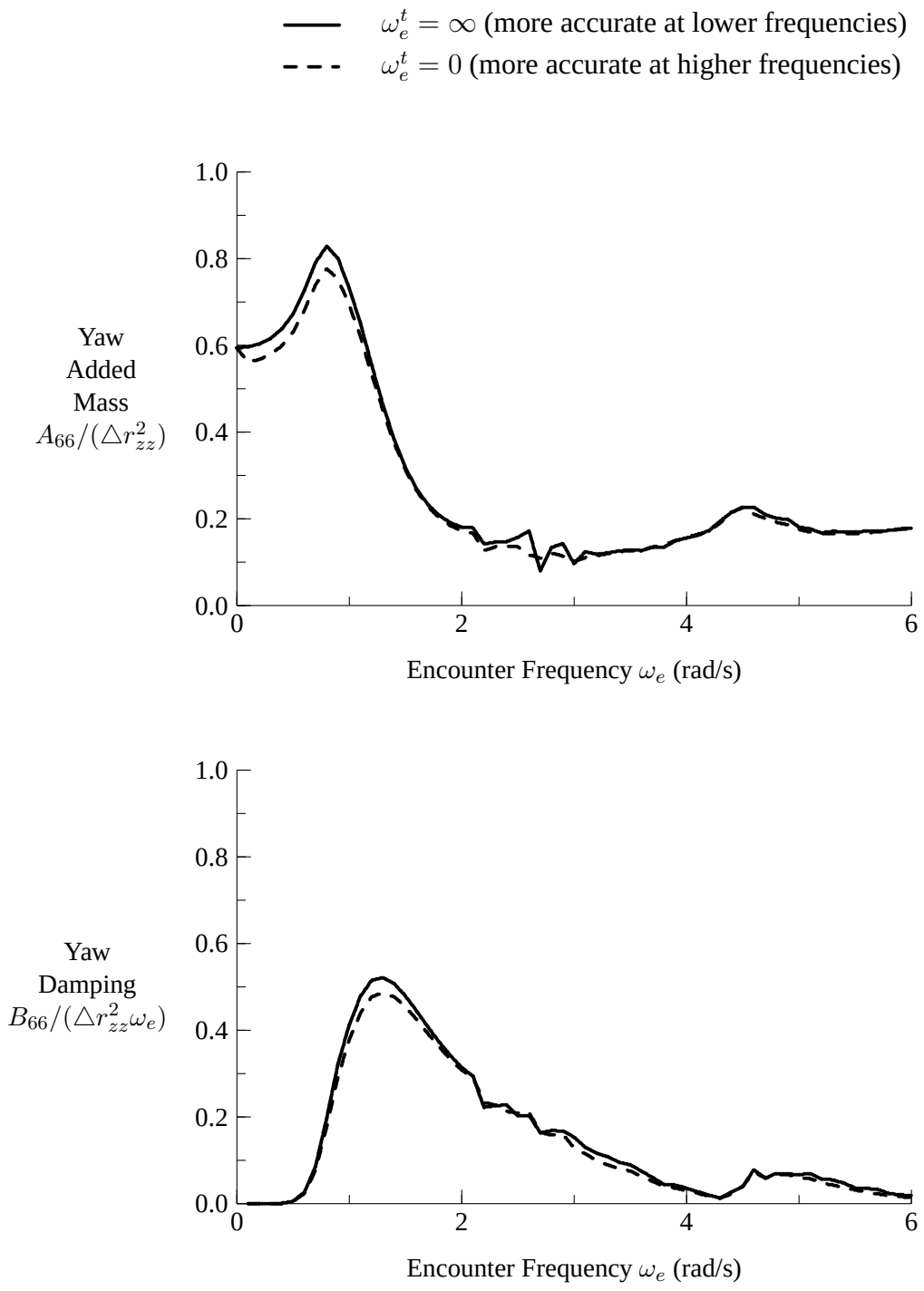

Figure 16: *Yaw Added Mass and Damping Coefficients for Coarse Mesh HALIFAX*

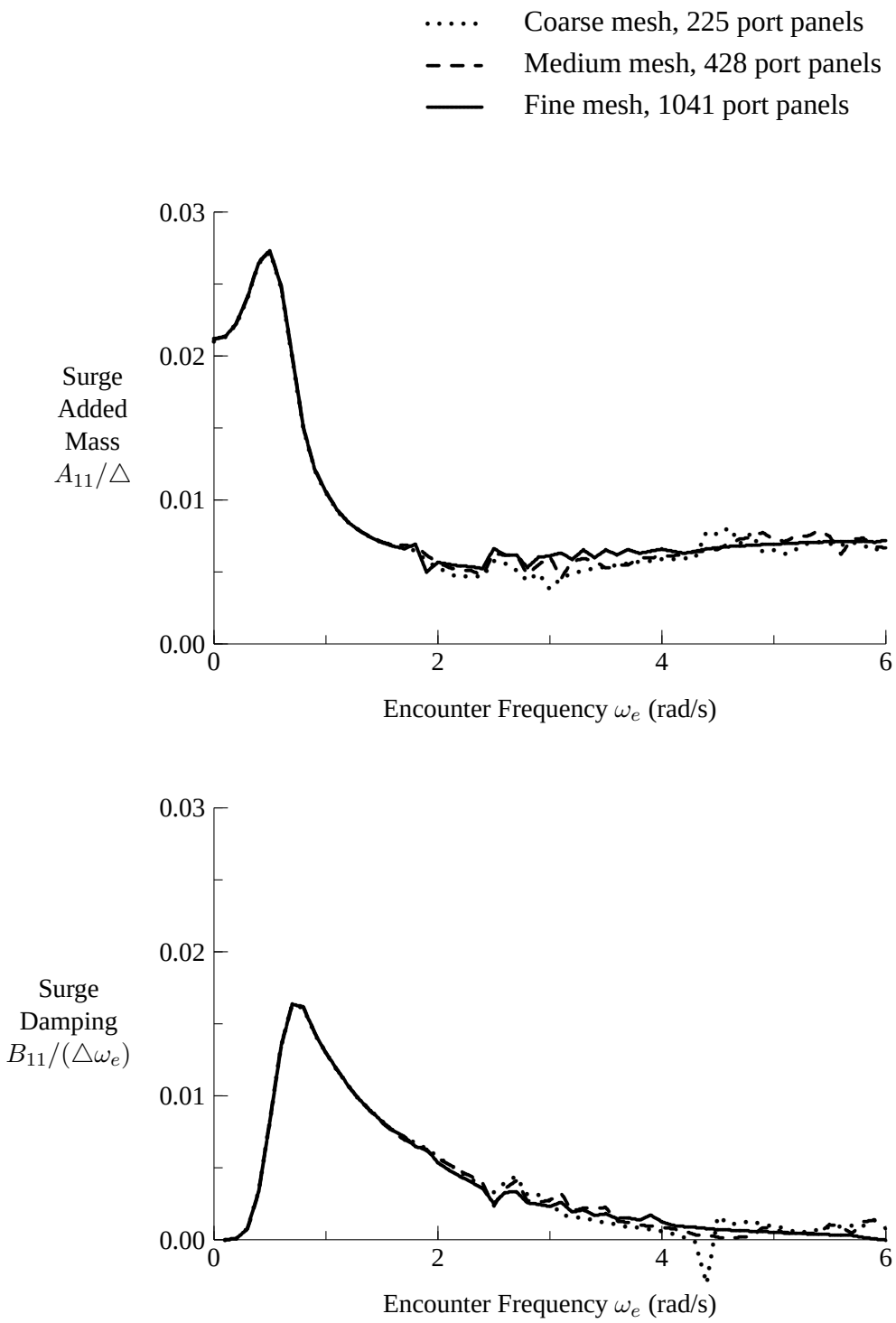

Figure 17: *Surge Added Mass and Damping Coefficients for HALIFAX*

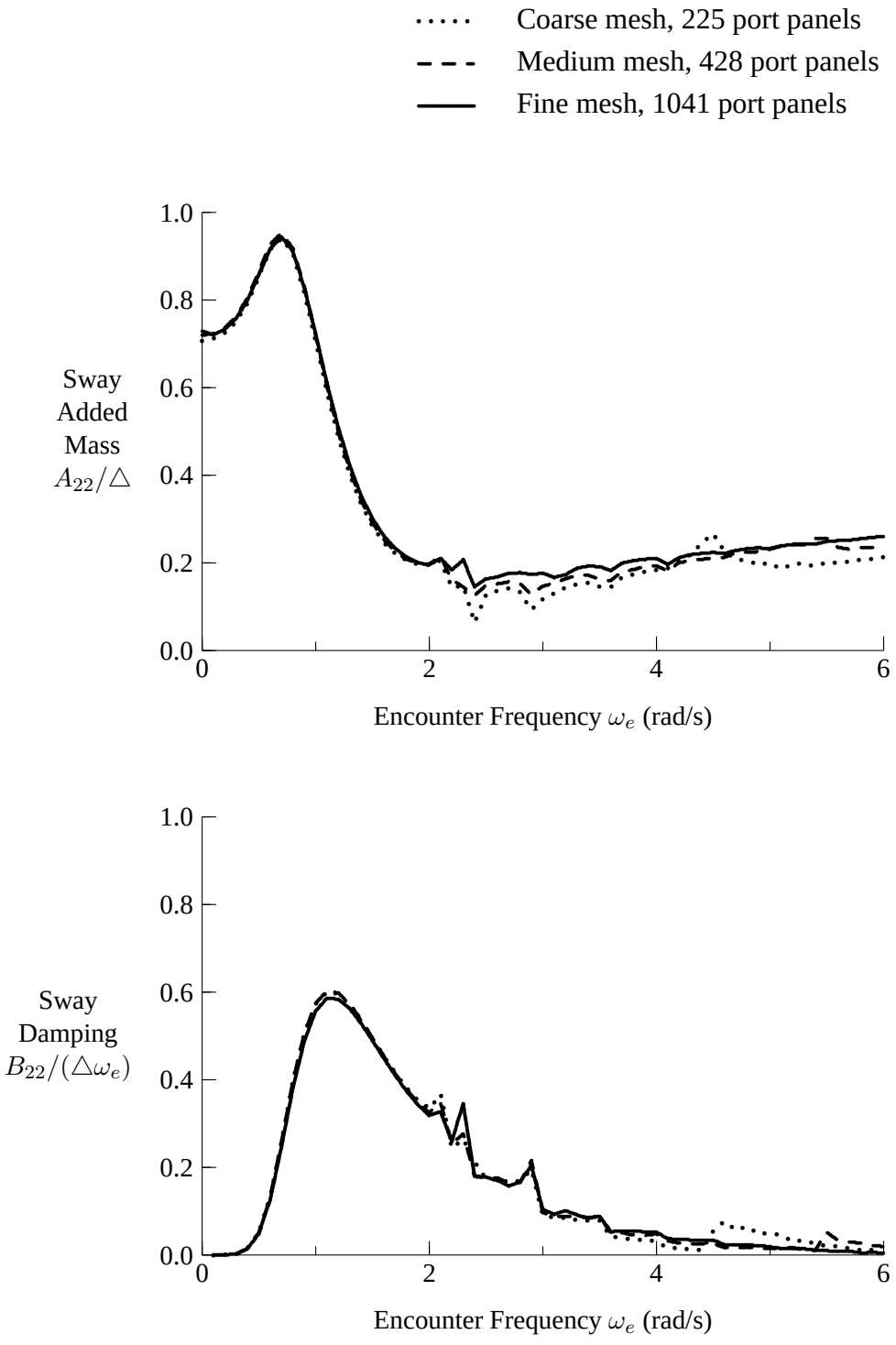

Figure 18: *Sway Added Mass and Damping Coefficients for HALIFAX*

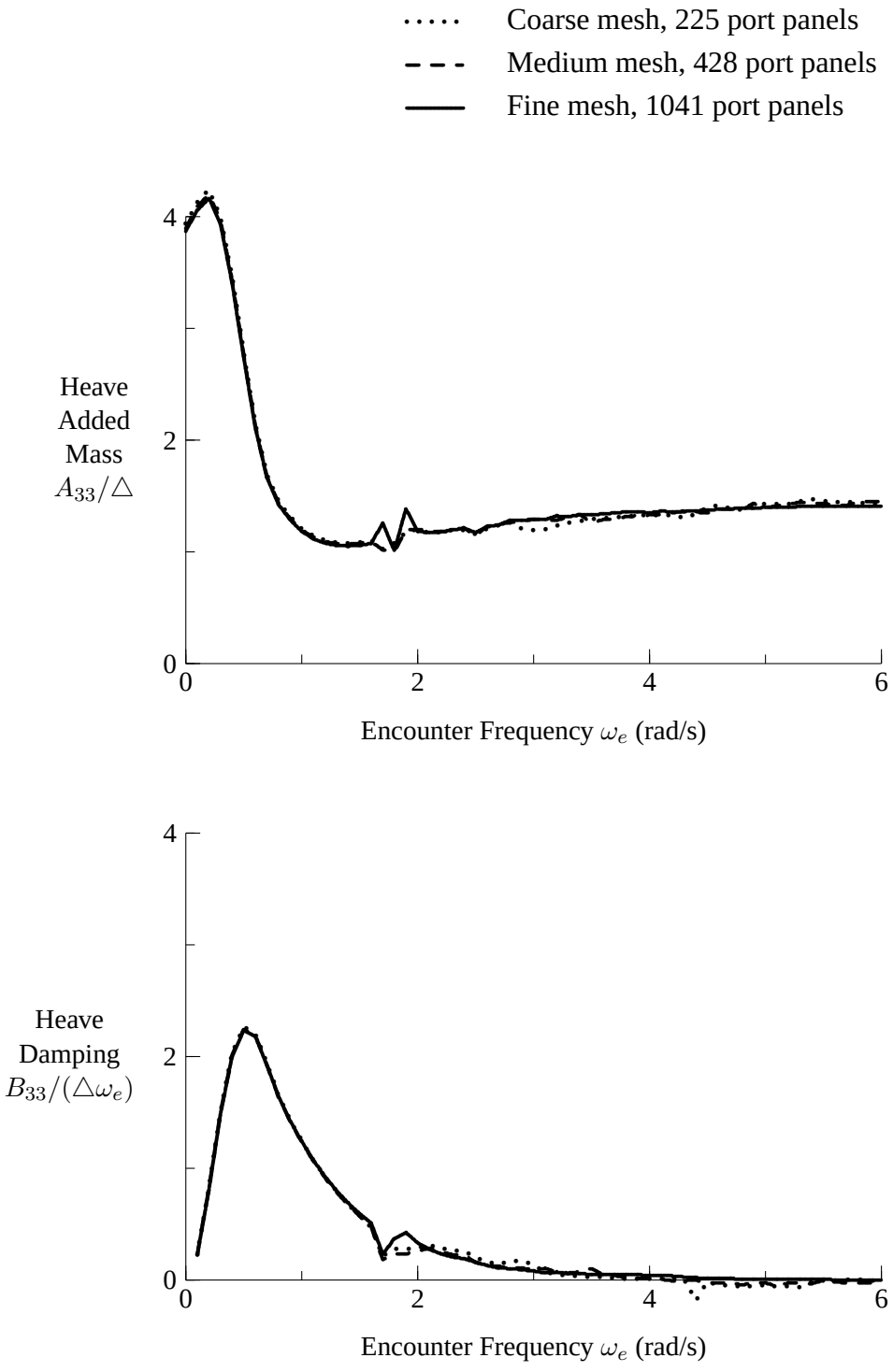

Figure 19: *Heave Added Mass and Damping Coefficients for HALIFAX*

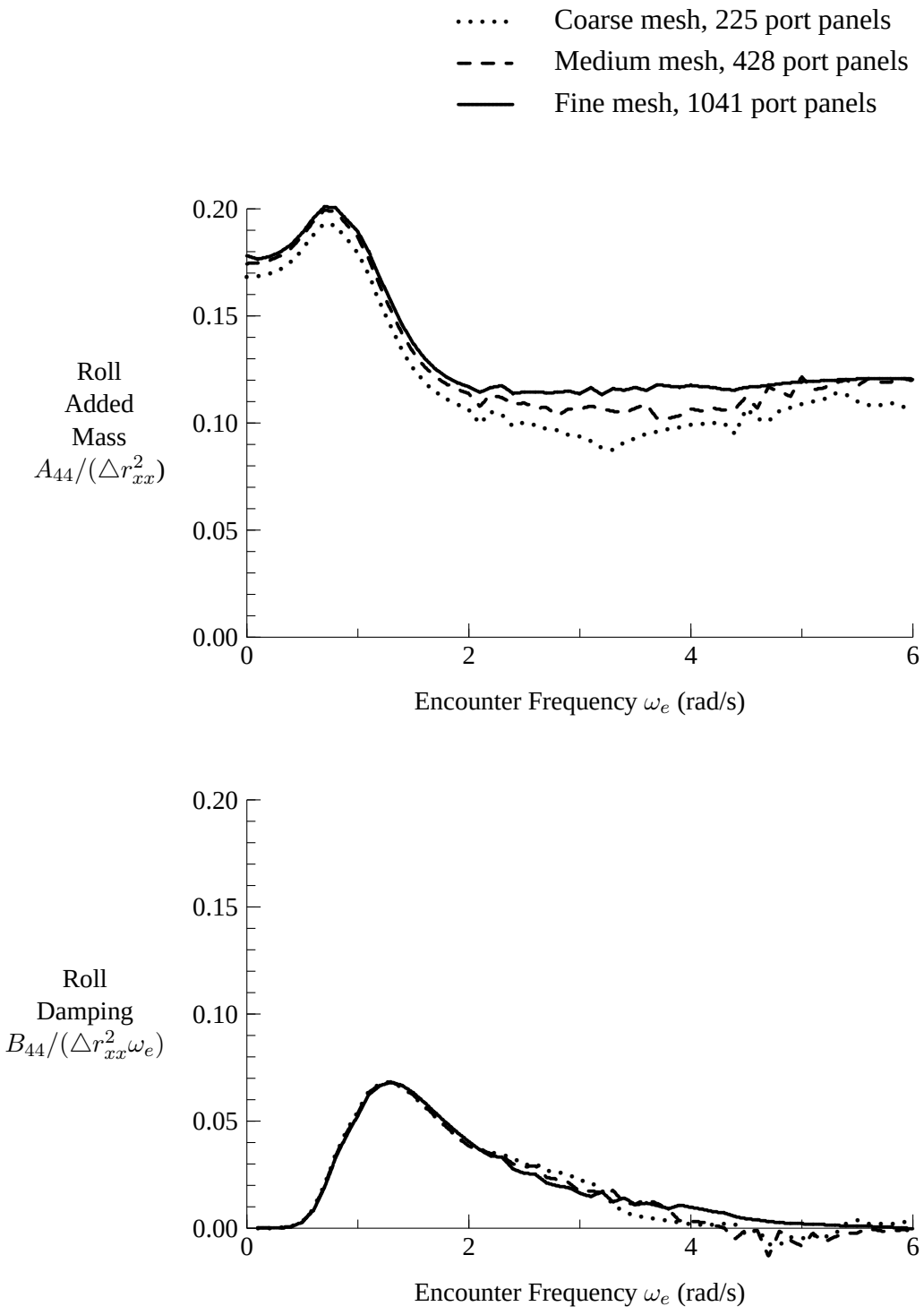

Figure 20: *Roll Added Mass and Damping Coefficients for HALIFAX*

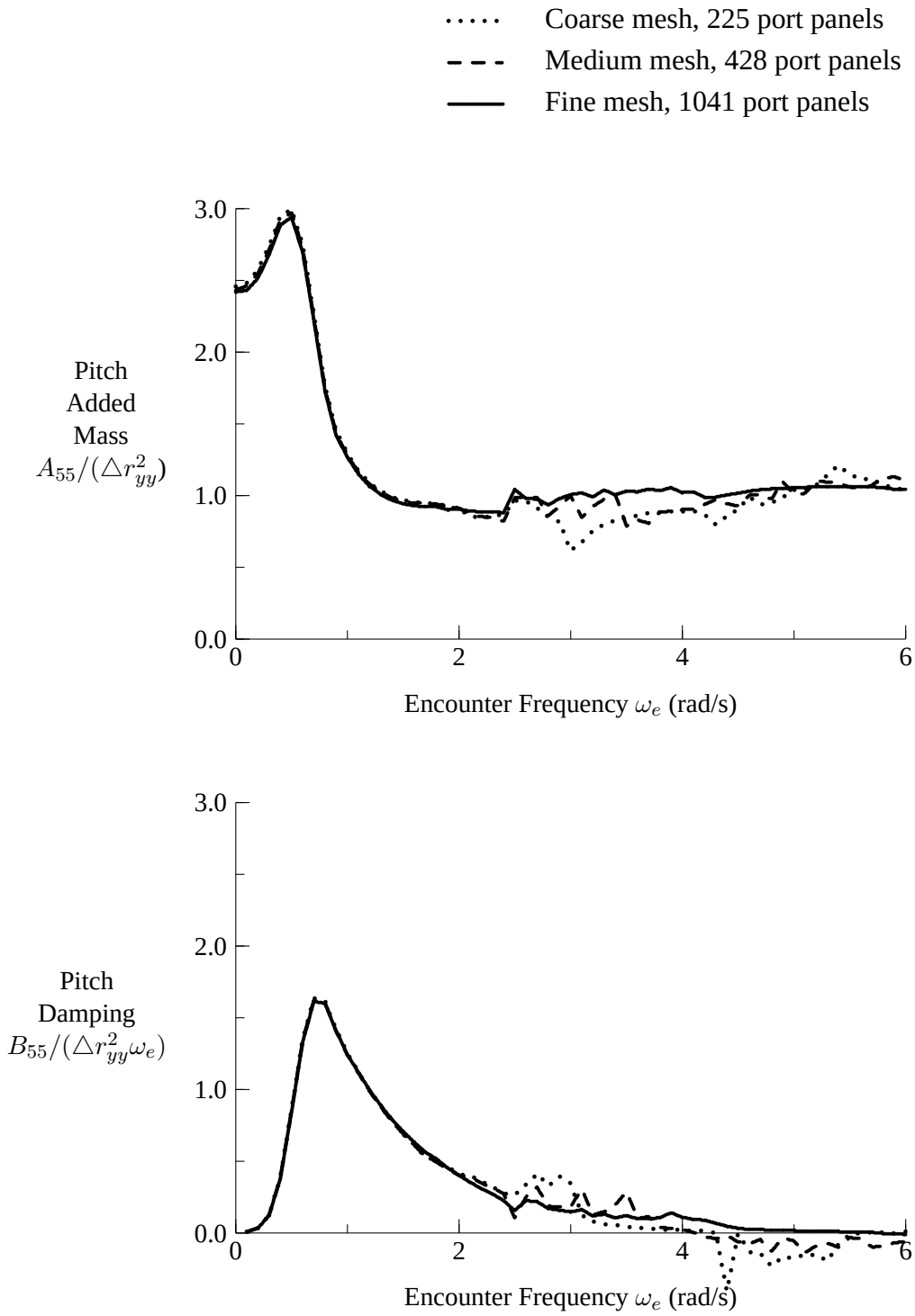

Figure 21: *Pitch Added Mass and Damping Coefficients for HALIFAX*

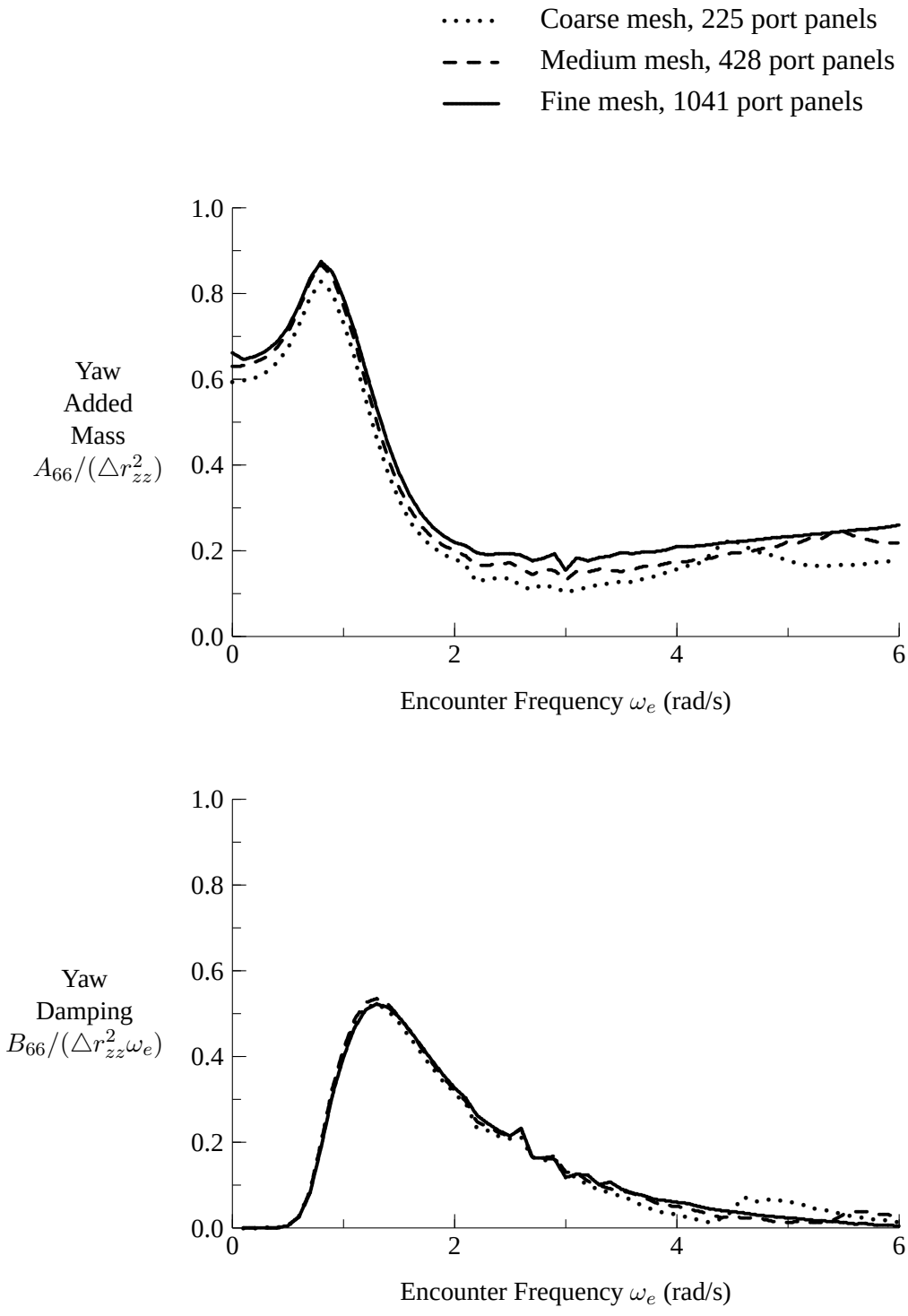

Figure 22: *Yaw Added Mass and Damping Coefficients for HALIFAX*

7.3 Motions in Waves

To verify the present computational methods, motions in waves have been computed for comparison with SHIPMO7 strip theory results. Three-dimensional predictions are based on potentials evaluated directly using Python class HullRadDiff and interpolated potentials using class HullRadDiffDB. For speed corrections with the three-dimensional predictions, the term U/ω_e has been assigned an upper limit of $L/2$. Figures 23 to 34 show predicted motions in waves for the HALIFAX class travelling at a speed of 18 knots in stern quartering (30 degrees) and bow quartering (150 degrees) waves. It has been found that 3D predictions from directly evaluated and interpolated potentials give virtually identical results; thus, the motions from interpolated potentials are not included in Figures 23 to 34.

The significant differences between 3D and SHIPMO7 strip theory predictions arise from several factors. Strip theory, and to a lesser extent the present 3D theory, is based on the assumption of high encounter frequency; thus, differences between the two approaches will be greater at low encounter frequencies. While strip theory codes often do not include surge motions, SHIPMO7 evaluates surge motions by assuming that surge diffraction forces are negligible. The SHIPMO7 predictions include viscous roll damping forces which aren't included in the present three-dimensional predictions. The most noticeable differences between the strip theory and three-dimensional predictions in Figures 23 to 34 are for surge and sway motions in stern quartering seas at a wave frequency of approximately 1.2 rad/s. At this combination of speed, heading, and wave frequency, encounter frequency is near zero, thus violating theoretical assumptions for both strip theory and the present 3D approach. It should be noted that SHIPMO7 alters wave frequencies to avoid computations at low encounter frequencies. For surge motions in stern quartering seas (Figure 23), diffraction forces could contribute to the differences between strip theory and 3D predictions. Significant differences in yaw motions occur at lower wave frequencies in both stern and bow quartering seas (Figures 33 and 34), and are likely due to three-dimensional effects.

Due to assumptions regarding high encounter frequency, the present results at forward ship speed for bow quartering seas provide the best basis for considering whether the current 3D approach has been correctly implemented. The very good agreement between strip theory and 3D theory for bow quartering seas (with the exception of yaw, as previously noted) verifies the implementation of the 3D theory. SHIPMO7 typically gives good agreement with experimental results in head and bow quartering seas [30, 31]; thus, the present computational results suggest that the three-dimensional theory will likely give very good agreement with experiments in bow quartering seas.

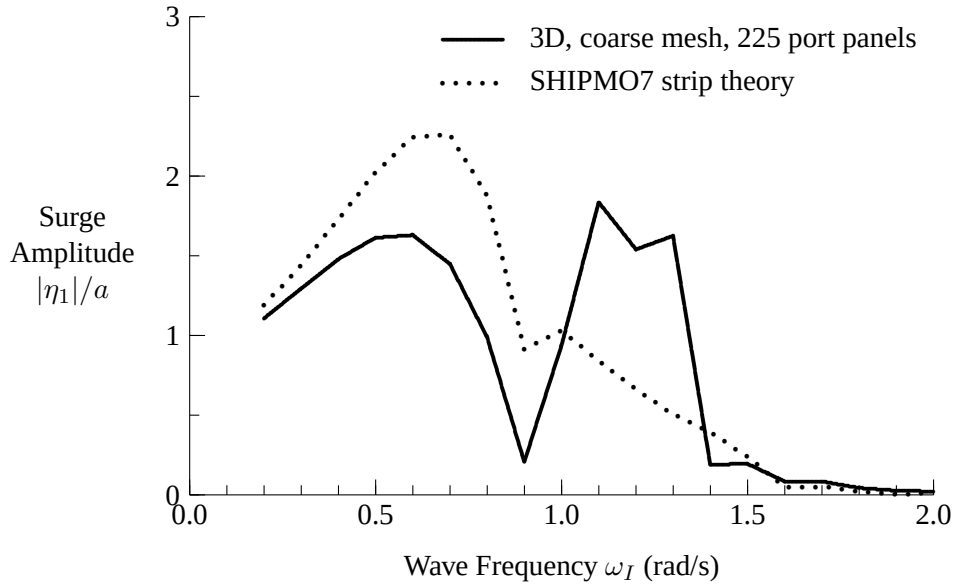

Figure 23: *HALIFAX Surge Motion in Stern Quartering Seas, 18 knots, 30 Degrees*

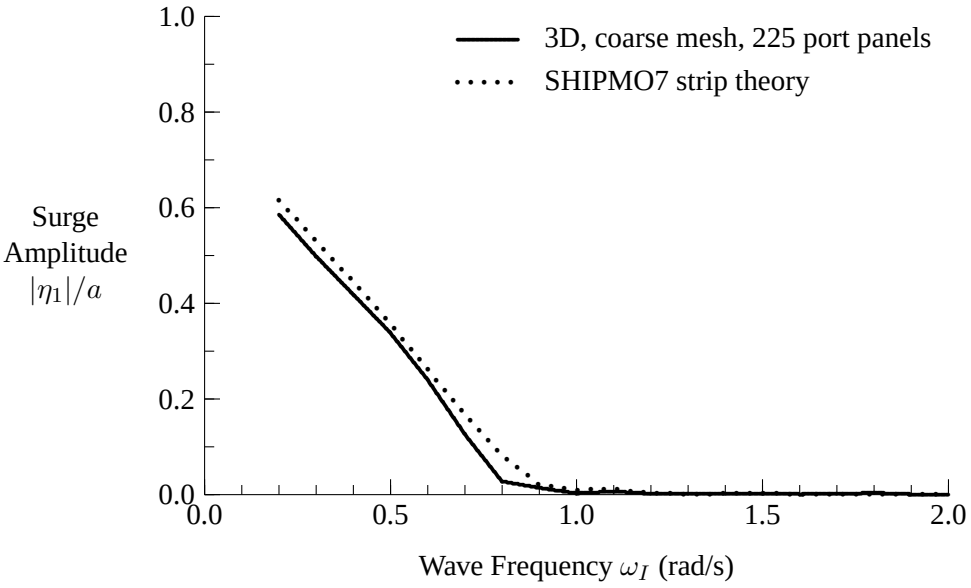

Figure 24: *HALIFAX Surge Motion in Bow Quartering Seas, 18 knots, 150 Degrees*

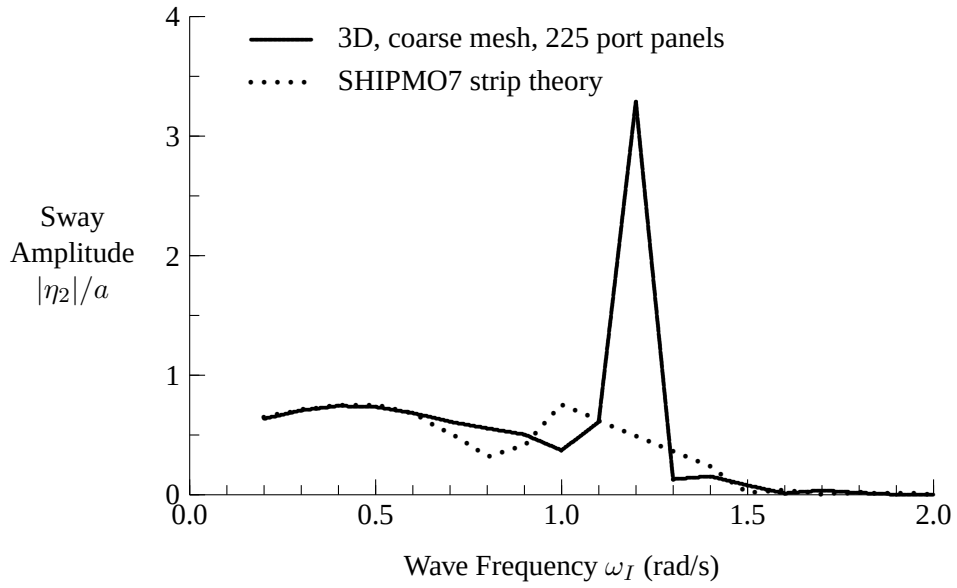

Figure 25: *HALIFAX Sway Motion in Stern Quartering Seas, 18 knots, 30 Degrees*

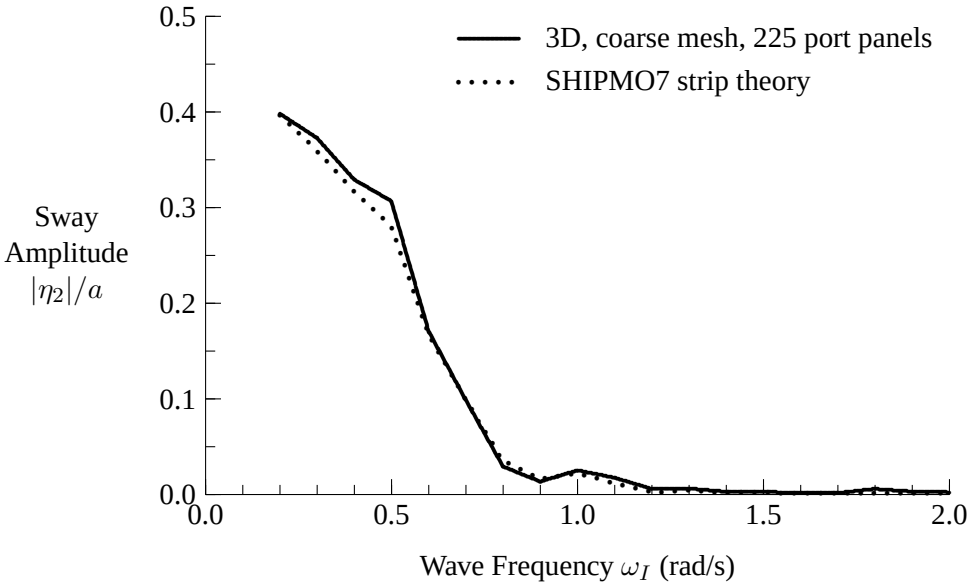

Figure 26: *HALIFAX Sway Motion in Bow Quartering Seas, 18 knots, 150 Degrees*

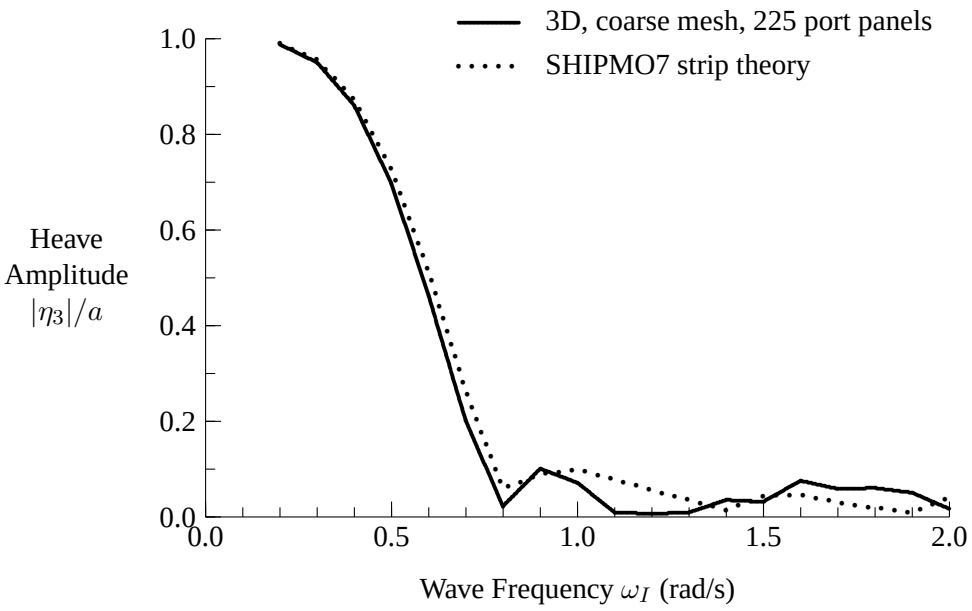

Figure 27: *HALIFAX Heave Motion in Stern Quartering Seas, 18 knots, 30 Degrees*

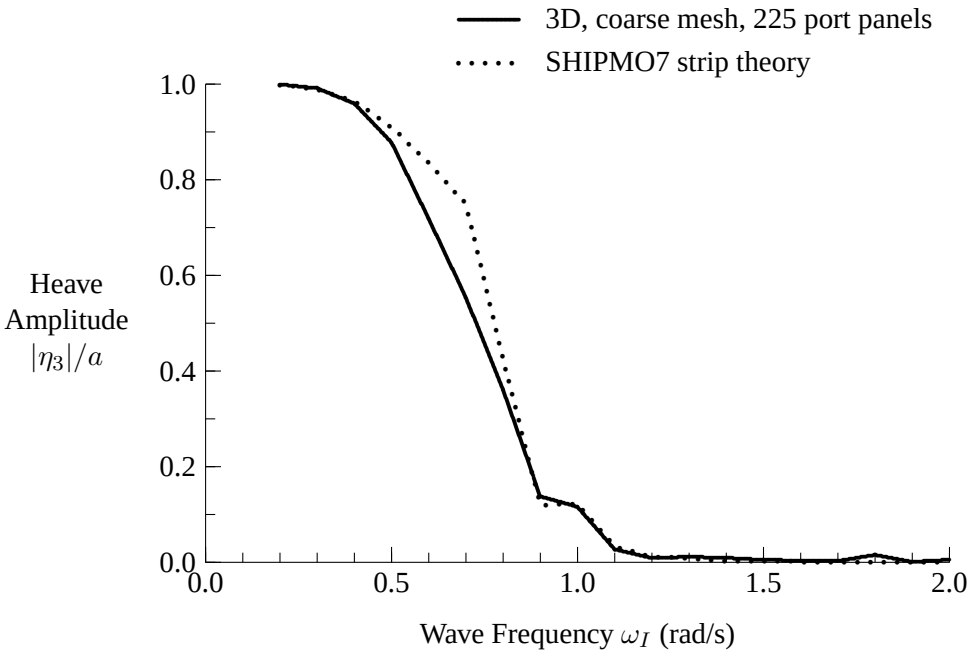

Figure 28: *HALIFAX Heave Motion in Bow Quartering Seas, 18 knots, 150 Degrees*

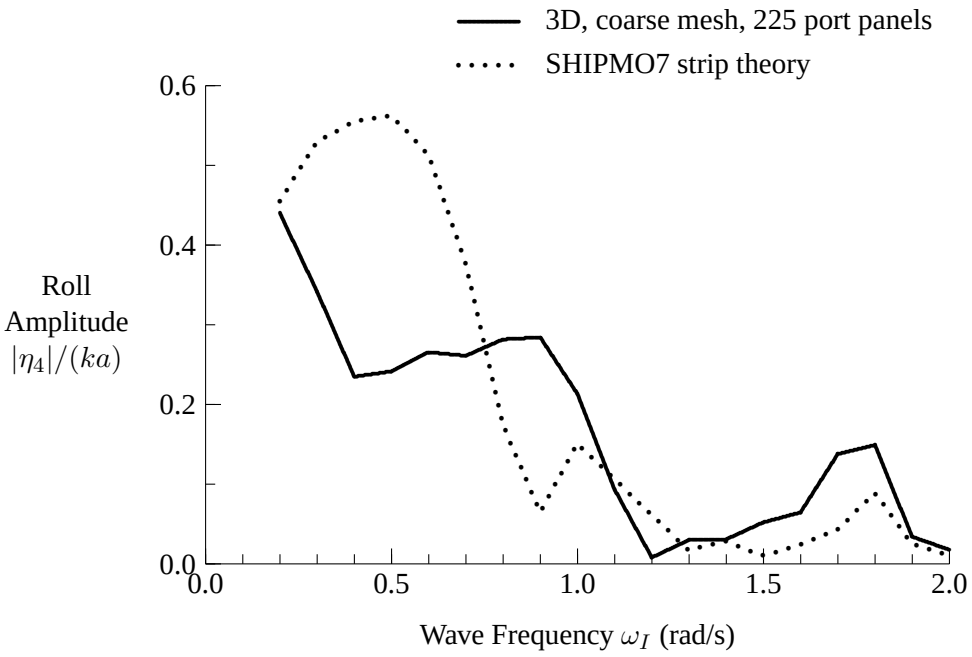

Figure 29: *HALIFAX Roll Motion in Stern Quartering Seas, 18 knots, 30 Degrees*

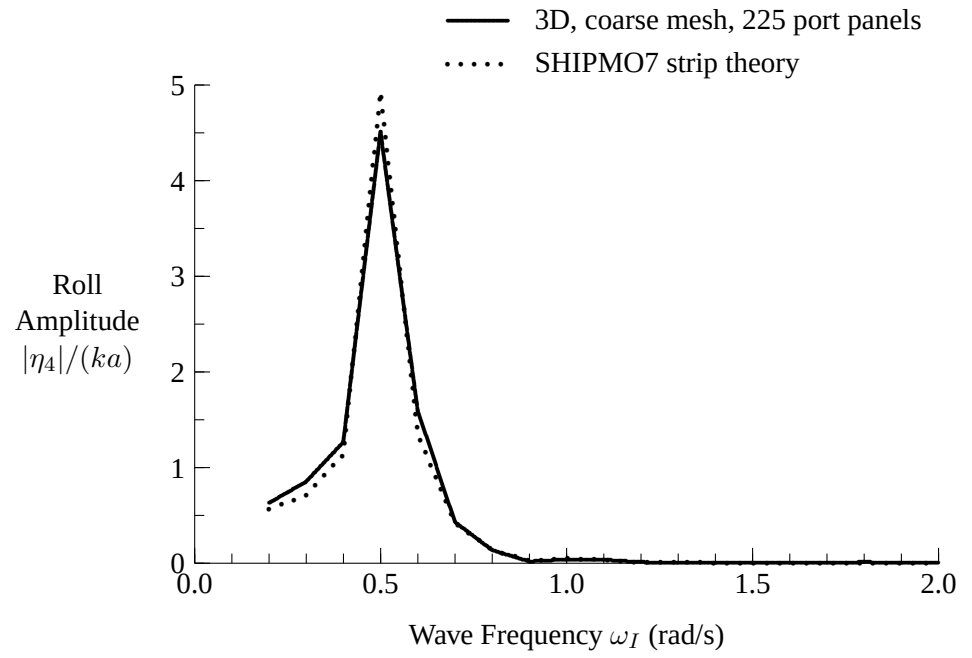

Figure 30: *HALIFAX Roll Motion in Bow Quartering Seas, 18 knots, 150 Degrees*

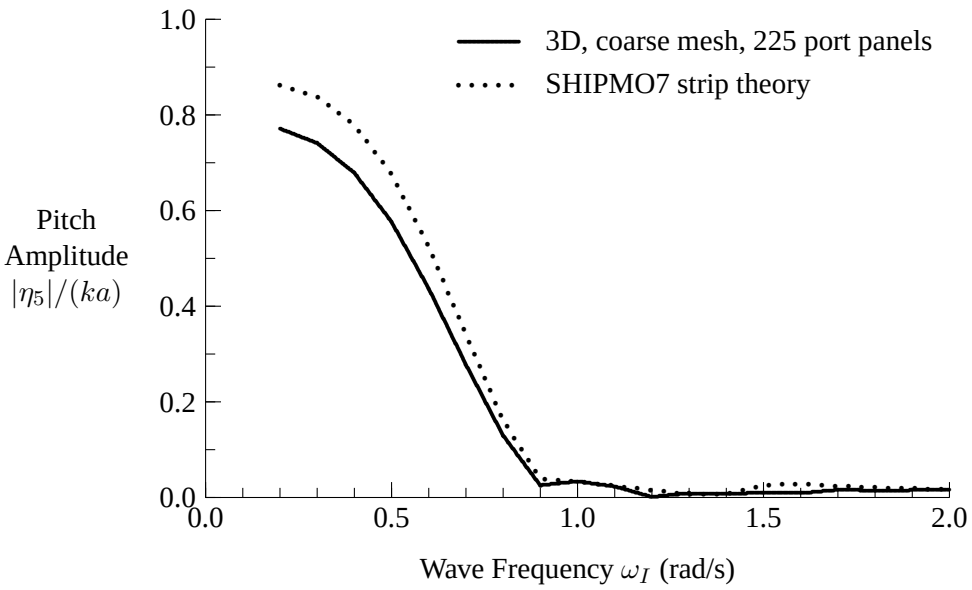

Figure 31: *HALIFAX Pitch Motion in Stern Quartering Seas, 18 knots, 30 Degrees*

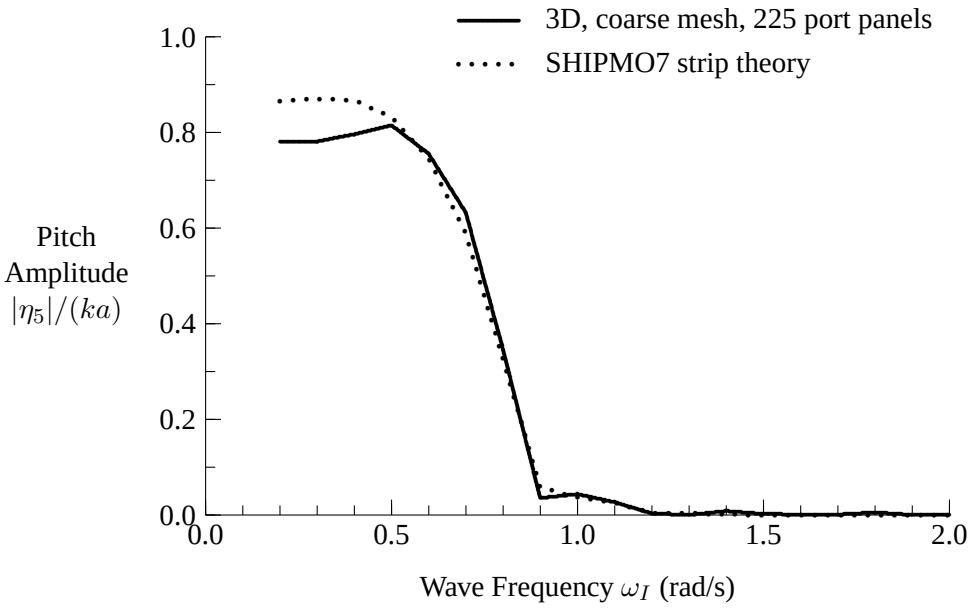

Figure 32: *HALIFAX Pitch Motion in Bow Quartering Seas, 18 knots, 150 Degrees*

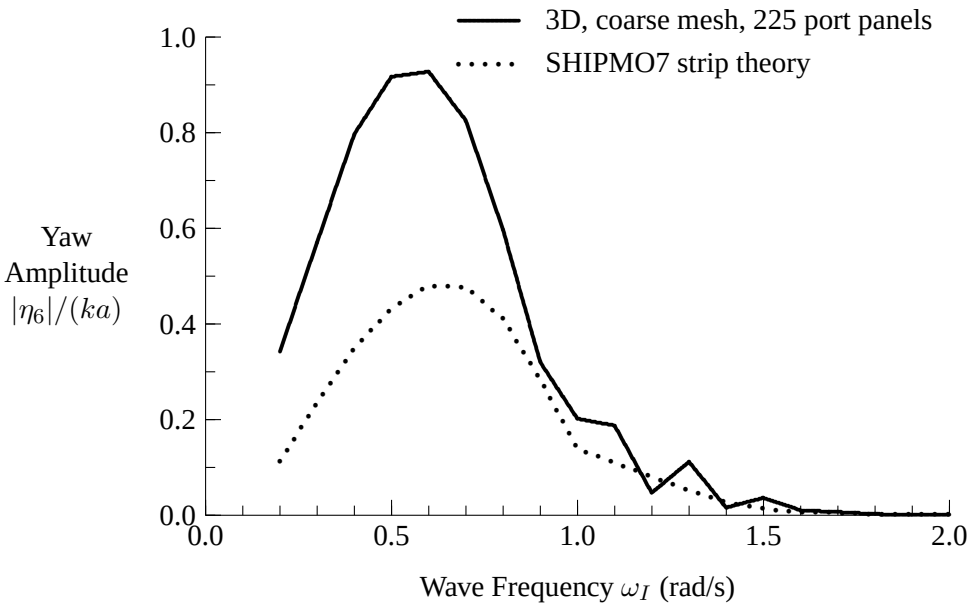

Figure 33: *HALIFAX Yaw Motion in Stern Quartering Seas, 18 knots, 30 Degrees*

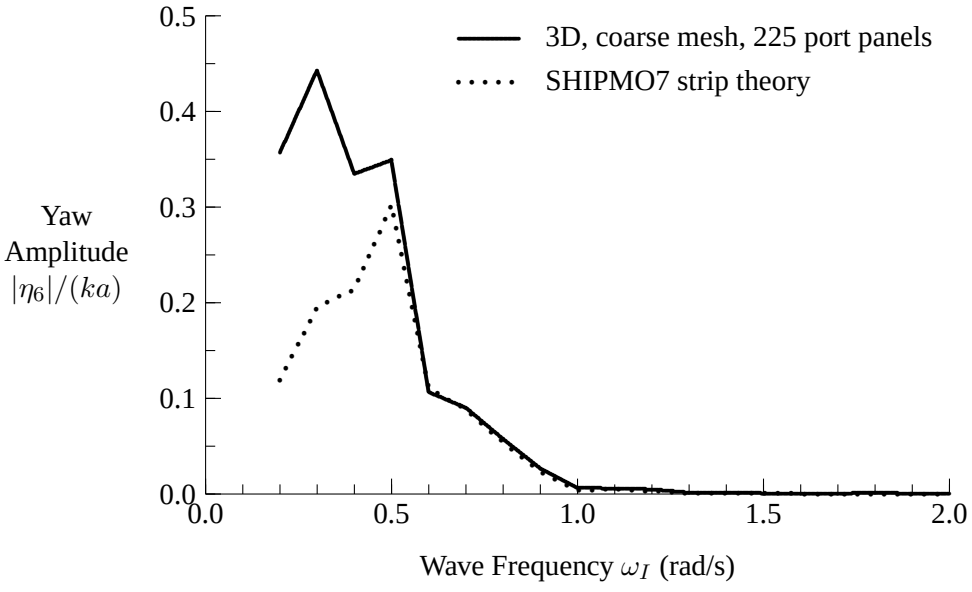

Figure 34: *HALIFAX Yaw Motion in Bow Quartering Seas, 18 knots, 150 Degrees*

7.4 Computational Requirements

Computational requirements are an important factor when considering the practical application of scientific computations. For the present computations using the HALIFAX coarse mesh (225 panels on half of hull), the required computer memory is approximately 60 MB. The amount of required memory will be approximately proportional to N_p^2, where N_p is the number of panels on the hull surface.

When evaluating ship motions using the hull potential database class HullRadDiffDB, almost all of the computational time is required for initialization. After the database has been initialized, radiation and diffraction forces can be obtained using negligible amounts of computational time. The database can be generated once for a given hull loading condition, and can be stored and reused for future computations using the Python "pickle" module (see Reference 26). The initialization time for the database class HullRadDiffDB depends on the number of panels, the number of encounter frequencies, and the number of seaways (i.e., combinations of ship speed, heading, and wave frequency) for diffraction computations. For the HALIFAX coarse mesh running on an 800 MHz Pentium III processor, approximately 45 seconds is required to generate a HullRadDiff object that is used as input to the database class HullRadDiffDB. Subsequent initialization computations require approximately 10 seconds per encounter frequency plus 5 seconds per seaway. A comprehensive database for a given ship loading condition can be developed using 50 input encounter frequencies, 6 ship speeds, 19 wave headings, and 20 wave frequencies (2280 seaway conditions), leading to a total initialization time of approximately 3 hours.

As mentioned above, a HullRadDiffDB object can be stored in a file for subsequent computations. When a HullRadDiffDB object is created, there is an option for retaining panel potentials, which are required for pressure and sea load computations. If hull potentials are not retained, then only the global ship hydrodynamic coefficients and forces need to be stored. The size of the file for storing a HullRadDiffDB object depends upon the number of encounter frequencies, number of seaways, number of hull panels, and whether panels potentials are to be retained. If hull potentials are not retained, then the storage file size is approximately 100 kB plus 4 kB per encounter frequency plus 0.5 kB per seaway. For our example case above of 50 encounter frequencies and 2280 seaway conditions, the size of the stored database file would be approximately 1.5 MB. If hull potentials are retained, the storage file size will increase significantly and be approximately proportional to the number of hull panels. For the HALIFAX coarse mesh, the storage file size is approximately 230 kB plus 120 kB per encounter frequency plus 80 kB per seaway. For our example case above of 50 encounter frequencies and 2280 seaway conditions, the size of the stored database file including panel potentials would be approximately 200 MB.

8 Conclusions

An efficient method has been developed for computing three-dimensional hydrodynamic coefficients in the frequency domain. This approach is based on the zero speed Green function, and includes extensions to include forward speed effects. Robustness and accuracy at both low and high frequency ranges are obtained by referencing the frequency dependent portion of the Green function to either the zero or infinite frequency Green function, depending on the encounter frequency. A new algorithm based on interpolated Green functions for computing radiation and diffraction potentials reduces the number of Green function evaluations when considering a variety of ship speeds, headings, and wave frequencies.

Sample computations for HALIFAX suggest that the approach gives reliable results for a coarse mesh with 225 panels on half of the ship. Computations with a fine mesh of 1041 panels appear to have somewhat better accuracy but require significantly more computational time. Comparisons of predicted motions with strip theory suggest that the new three-dimensional method is giving reliable results.

References

1. McTaggart, K.A. (1997). SHIPMO7: An Updated Strip Theory Program for Predicting Ship Motions and Sea Loads in Waves. (DREA TM 96/243). Defence Research Establishment Atlantic.

2. SeaTech, BMT (1995). User's Manual for Motion, Load and Pressure Program Suite - PRECAL. Technical Report. prepared for NSMB CRS PRECAL Working Group. Distribution limited to CRS members.

3. McTaggart, K.A. and Stredulinsky, D. (2001). Comparisons of Motions for HMCS NIPIGON with Numerical Predictions. (DREA ECR 2001-156). Defence Research Establishment Atlantic.

4. Schmitke, R.T. (1978). Ship Sway, Roll, and Yaw Motions in Oblique Seas. *Transactions, Society of Naval Architects and Marine Engineers*, **86**, 26–46.

5. McTaggart, K.A. (2000). Lateral Ship Motions and Sea Loads in Waves Including Appendage and Viscous Forces. *International Shipbuilding Progress*, **47**(450), 141–160.

6. Beck, R.F. and Loken, A.E. (1989). Three-Dimensional Effects in Ship Relative-Motion Probelms. *Journal of Ship Research*, **33**(4), 261–268.

7. Papanikolaou, A.D. and Schellin, T.E. (1992). A Three-Dimensional Panel Method for Motions and Loads of Ships with Forward Speed. *Schiffstechnik (Ship Technology Research)*, **39**, 147–156.

8. Hsiung, C.C. and Huang, Z.J. (1995). Final Report: The Frequency-Domain Prediction of Added Resistance of Ships in Waves Using a Near-Field, 3-Dimensional Flow Method. (CR/95/484). Defence Research Establishment Atlantic.

9. Faltinsen, O.M. and Michelsen, F.C. (1974). Motions of Large Structures in Waves at Zero Froude Number. In *The Dynamics of Marine Vehicles and Structures in Waves*, London.

10. Hogben, N. and Standing, R.G. (1974). Wave Loads on Large Bodies. In *The Dynamics of Marine Vehicles and Structures in Waves*, London.

11. Garrison, C.J. (1978). Hydrodynamic Loading of Large Offshore Structures. In Zienkiewicz, O.C., Lewis, O.C., and Stagg, K.G., (Eds.), *Numerical Methods in Offshore Engineering*, pp. 87–139. Chichester, England: John Wiley & Sons.

12. Sarpkaya, T. and Isaacson, M. (1981). Mechanics of Wave Forces on Offshore Structures, Van Nostrand Reinhold.

13. Newman, J.N. (1985). The Evaluation of Free-Surface Green Functions. In *Fourth International Conference on Numerical Ship Hydrodynamics*, Washington.

14. S.K.Chakrabarti (2001). Application and Verification of Deepwater Green Function for Water Waves. *Journal of Ship Research*, **45**(3), 187–196.

15. Telste, J.G. and Noblesse, F. (1986). Numerical Evaluation of the Green Function of Water-Wave Radiation and Diffraction. *Journal of Ship Research*, **30**(2), 69–84.

16. Salvesen, N., Tuck, E.O., and Faltinsen, O. (1970). Ship Motions and Sea Loads. *Transactions, Society of Naval Architects and Marine Engineers*, **78**, 250–287.

17. Huang, Z.J. and Hsiung, C.C. (1993). An Improved 3-D Panel Method to Compute mj-Terms for Ship Motion. In *Proceedings of the Second Canadian Marine Dynamics Conference*, Vancouver.

18. Inglis, R.B. and Price, W.G. (1981). Calculation of the Velocity Potential of a Translating, Pulsating Source. *Transactions, Royal Institution of Naval Architects*, **123**, 163–175.

19. Ba, M. and Guilbaud, M. (1995). A Fast Method of Evaluation for the Translating and Pulsating Green's Function. *Schiffstechnik (Ship Technology Research)*, **42**, 68–80.

20. Hess, J.L. and Smith, A.M.O. (1964). Calculation of Nonlifting Potential Flow About Arbitrary Three-Dimensional Bodies. *Journal of Ship Research*, **8**(3), 22–44.

21. Hally, D. (1989). POTFLO: A Suite of Programs for Calculating Potential Flow about Ship Hulls. (DREA TM 89/210). Defence Research Establishment Atlantic.

22. Hally, D. (1992). HLLSPL User's Guide: A Program for Generating HLLSRF Representations of Ship Hulls. (DREA TC 92/310). Defence Research Establishment Atlantic.

23. Hally, D. (1993). User's Guide for HLLFLO Version 2.0. (DREA TC 93/309). Defence Research Establishment Atlantic.

24. Hally, D. (1994). Integration of the Wave Resistance Green Function Over Planar Panels. (DREA TM 94/206). Defence Research Establishment Atlantic.

25. Lutz, M. (2001). Programming Python, Second ed. Sebastopol, CA: O'Reilly & Associates.

26. Lutz, M. and Ascher, D. (1999). Learning Python, Sebastopol, CA: O'Reilly & Associates.

27. Ascher, D., Dubois, P.F., Hinsen, K., Hugunin, J., and Oliphant, T. (2001). Numerical Python. (Technical Report UCRL-MA-128569). Lawrence Livermore National Laboratory. Livermore, California.

28. McTaggart, K.A. (1996). Improved Boundary Element Methods for Predicting Sectional Hydrodynamic Coefficients for Strip Theory Ship Motion Programs. (DREA TM 96/212). Defence Research Establishment Atlantic.

29. Ando, S. (2002). Lower Bounds to Irregular Frequencies in Wave-Ship Interactions for Engineering Applications. (DREA TM 2001-192). Defence Research Establishment Atlantic.

30. Chow, D.L. and McTaggart, K.A. (1996). Validation of SHIPMO7 and PRECAL Predictions with a Warship Model. (DREA TM 97/203). Defence Research Establishment Atlantic.

31. McTaggart, K.A. and Chow, D.L. (1997). Validation of SHIPMO7 and PRECAL Predictions with the CPF Hydroelastic Model. (DREA TM 97/216). Defence Research Establishment Atlantic.

Symbols

$[A]$	added mass matrix
A_j	area of panel j
A_s	source area
A_{wp}	waterplane area
a	wave amplitude
B	ship beam
b	aspect ratio of rectangular panel
$[C]$	hydrodynamic stiffness matrix
$[D]$	normal flow velocity influence matrix
$[E]$	velocity potential influence matrix
$\{F_D\}$	diffracted wave force vector
$\{F_I\}$	incident wave force vector
G	Green function
$\overline{G}_0$	zero frequency Green function
$\widetilde{G}_0$	frequency dependent term of Green function relative to zero frequency Green function
$\widetilde{G}_\infty$	frequency dependent term of Green function relative to infinite frequency Green function
g	gravitational acceleration
$[H]$	x velocity influence matrix
h	non-dimensional horizontal distance from field point to source
I_{wp-xx}	x moment of waterplane area
I_{wp-yy}	y moment of waterplane area
$J_0(h)$	Bessel function of the first kind of order zero
$J_1(h)$	Bessel function of the first kind of order one
$\overline{KG}$	centre of gravity above baseline
k_e	encounter wavenumber
k_I	incident wavenumber
L	ship length between perpendiculars
$[M]$	inertial matrix
n_k	outward normal component k
N_e	number of encounter frequencies
N_G	number of evaluations of Green function
N_p	number of panels
p	pressure
$port$	superscript denoting port side of hull
R	distance from field point to source
R_{xy}	horizontal distance from field point to source

$\widetilde{R_0}(h,v)$	term for evaluation of frequency dependent Green function
R_1	distance from field point to source image
$\widetilde{R_1}(h,v)$	term for evaluation of frequency dependent Green function
r_{xx}	roll radius of gyration
r_{yy}	pitch radius of gyration
r_{zz}	yaw radius of gyration
S_b	surface of floating body
S_k	surface of hull panel k
S_s	surface of source
$star$	superscript denoting starboard side of hull
T_{mid}	draft at midships
t_s	trim by stern
U	ship speed
v	non-dimensional vertical distance from field point to source image
v_n	normal flow velocity
$\vec{x}$	location in space
$\vec{x}_s$	source location
$\vec{x}_{sc}$	source centroid location
x_{wp}	x coordinate of centre of floatation
x_{CB}	x coordinate of centre of gravity
z_{CB}	z coordinate of center of buoyancy
z_{CG}	z coordinate of center of gravity
β	wave direction relative to ship
δ_{jk}	Kroenecker delta function
ζ_3	oscillatory vertical displacement
η_j	motion amplitude in mode j
ρ	water density
σ	source strength
Φ	total oscillatory velocity potential
ϕ_D	diffracted wave potential
ϕ_I	incident wave potential
ϕ_j	radiated wave potential due to motion mode j
ω_I	incident wave frequency
ω_e	wave encounter frequency
ω_e^t	transition encounter frequency for Green function computation
$\bigtriangledown$	ship volume
$\bigtriangleup$	ship mass displacement

This page intentionally left blank.

DOCUMENT CONTROL DATA

(Security classification of title, body of abstract and indexing annotation must be entered when document is classified)

1. ORIGINATOR (the name and address of the organization preparing the document. Organizations for whom the document was prepared, e.g. Centre sponsoring a contractor's report, or tasking agency, are entered in section 8.)

Defence R&D Canada - Atlantic

2. SECURITY CLASSIFICATION (overall security classification of the document including special warning terms if applicable).

UNCLASSIFIED

3. TITLE (the complete document title as indicated on the title page. Its classification should be indicated by the appropriate abbreviation (S,C,R or U) in parentheses after the title).

Three Dimensional Ship Hydrodynamic Coefficients Using the Zero Forward Speed Green Function

4. AUTHORS (Last name, first name, middle initial. If military, show rank, e.g. Doe, Maj. John E.)

McTaggart, Kevin A.

5. DATE OF PUBLICATION (month and year of publication of document)

April 2002

6a. NO. OF PAGES (total including Annexes, Appendices, etc).

66

6b. NO. OF REFS (total cited in document)

31

7. DESCRIPTIVE NOTES (the category of the document, e.g. technical report, technical note or memorandum. If appropriate, enter the type of report, e.g. interim, progress, summary, annual or final. Give the inclusive dates when a specific reporting period is covered).

Technical Memorandum

8. SPONSORING ACTIVITY (the name of the department project office or laboratory sponsoring the research and development. Include address).

Defence R&D Canada - Atlantic, PO Box 1012, Dartmouth, NS, Canada B2Y 3Z7

9a. PROJECT OR GRANT NO. (if appropriate, the applicable research and development project or grant number under which the document was written. Please specify whether project or grant).

11GK

9b. CONTRACT NO. (if appropriate, the applicable number under which the document was written).

10a. ORIGINATOR'S DOCUMENT NUMBER (the official document number by which the document is identified by the originating activity. This number must be unique.)

DRDC Atlantic TM 2002-059

10b. OTHER DOCUMENT NOs. (Any other numbers which may be assigned this document either by the originator or by the sponsor.)

11. DOCUMENT AVAILABILITY (any limitations on further dissemination of the document, other than those imposed by security classification)

(X) Unlimited distribution

( ) Defence departments and defence contractors; further distribution only as approved
( ) Defence departments and Canadian defence contractors; further distribution only as approved
( ) Government departments and agencies; further distribution only as approved
( ) Defence departments; further distribution only as approved
( ) Other (please specify):

12. DOCUMENT ANNOUNCEMENT (any limitation to the bibliographic announcement of this document. This will normally correspond to the Document Availability (11). However, where further distribution (beyond the audience specified in (11) is possible, a wider announcement audience may be selected).

13. ABSTRACT (a brief and factual summary of the document. It may also appear elsewhere in the body of the document itself. It is highly desirable that the abstract of classified documents be unclassified. Each paragraph of the abstract shall begin with an indication of the security classification of the information in the paragraph (unless the document itself is unclassified) represented as (S), (C), (R), or (U). It is not necessary to include here abstracts in both official languages unless the text is bilingual).

This report presents a method for predicting ship hydrodynamic coefficients and pressures in waves. Computations are performed in the frequency domain using the Green function for zero forward speed. Pressures and coefficients at non-zero forward speed are computed using extensions to zero speed results. The approach has been implemented using the Python programming language. The present implementation gives robust results over a wide range of wave frequencies. A new algorithm facilitates efficient computation of hydrodynamic terms for a large number of combinations of ship speed, heading, and incident wave frequency. Sample computations for the HALIFAX class demonstrate application of the method.

14. KEYWORDS, DESCRIPTORS or IDENTIFIERS (technically meaningful terms or short phrases that characterize a document and could be helpful in cataloguing the document. They should be selected so that no security classification is required. Identifiers, such as equipment model designation, trade name, military project code name, geographic location may also be included. If possible keywords should be selected from a published thesaurus. e.g. Thesaurus of Engineering and Scientific Terms (TEST) and that thesaurus-identified. If it not possible to select indexing terms which are Unclassified, the classification of each should be indicated as with the title).

heave
panel methods
pitch
roll
sea loads
seakeeping
ship motions
surge
sway
yaw

Defence R&D Canada
is the national authority for providing
Science and Technology (S&T) leadership
in the advancement and maintenance
of Canada's defence capabilities.

R & D pour la défense Canada
est responsable, au niveau national, pour
les sciences et la technologie (S & T)
au service de l'avancement et du maintien des
capacités de défense du Canada.

www.drdc-rddc.gc.ca